

4. McCLURE, D.S.: Solid State Phys, Vol. 9, p. 399 (eds. F. Seitz and D. Turnbull). New York: Academic Press 1959.
5. ROACH, P.R., ABRAHAM, B.N., KETTERSON, J.B., GREINER, R., VAN ANTWERP, W.: J. Low Temp. Phys. **13**, 59 (1973).
6. LEBESQUE, J.V., SNEL, J., SMIT, J.J.: Sol. State Comm. **13**, 371 (1973).
7. SMIT, J., WUN, H.P.J.: Ferrites. New York: John Wiley and Sons 1959.
8. SLONCZEWSKI, J.C.: Phys. Rev. **110**, 1341 (1958).
9. CHIN, G.Y.: Bell Lab. Record **49**, 71 (1971).
10. WERNICK, J.H.: Ann. Rev. Mat. Sci., Vol.2, p.607 (ed. R.A. HUGGINS). Palo Alto, Calif.: Annual Reviews Inc. 1972.
11. MORTON, J.A.: Trans. I.E.E.E. MAG-7, 333 (1971).
12. BOBECK, A.H., SCOVIL, H.E.D.: Sci. Am. **224**, 78 (1971).
13. HUDSON, A.H.: Revs. Phys. in Tech. **1**, 9 (1970).
14. COHEN, R.W., MEZRICH, R.S.: R. C. A. Review **33**, 54 (1972).
15. ANDERSON, L.K.: J. Appl. Phys. **34**, 1230 (1963).
16. BERTAUT, E.F., MERCIER, M.: Mat. Res. Bull. **6**, 907 (1971).
17. GOSHEN, S., MUKAMEL, D., SHAKED, H.: J. Appl. Phys. **40**, 1590 (1969).

VII. Materials with Useful Mechanical Properties

Inorganic solids are not very elastic. Cohesive strengths are typically 1% of the elastic modulus, which means that the solid elongates only a few percent before breaking. Elastic properties of oxides are nevertheless important in ceramic science and in the geosciences. Most minerals in the earth's crust are oxides and their stiffness moduli bear special relevance to our understanding of rock mechanics and seismic wave velocities. Recent developments in acousto-optics and surface waves have also generated interest in the elastic properties of oxides. New materials with unusual elastic behavior are needed for delay-lines and other electronic devices in which an electric signal is converted to an acoustic wave and subsequently re-converted to an electric signal. Elastic coefficients govern the velocity of the acoustic wave, and hence the transit time.

1. Elasticity

All solids change shape under forces. Under small stress, the strain ϵ is related to the stress σ by Hooke's law ($\sigma = (c)\epsilon$). The elastic stiffness coefficients (c) constitute a fourth rank tensor in which the number of independent coefficients depends on symmetry (Table 4). In concentrated matrix notation $\sigma_i = c_{ij}\epsilon_j$, where $i, j = 1, 2, 3$ refer to longitudinal stresses and strains along axes X_1 , X_2 , and X_3 , respectively. For shearing motions about each of the axes, $i, j = 4, 5, 6$. The discussion which follows will be concerned mainly with the relative values of c_{11} , c_{22} , and c_{33} , the coefficients relating change in length along a principal direction to a parallel component of stress. The shearing stiffness about the three principal axes are c_{44} , c_{55} , and c_{66} .

Stiffness coefficients for many inorganic materials have been collected by HEARMON [1], SIMMONS [2], and HUNTINGDON [3]. From the results it appears that packing density is the primary variable affecting the elastic moduli of oxide compounds. BIRCH [4, 5] has shown that most common minerals have about the same mean atomic weight (molecular weight divided by the number of atoms in the chemical formula), and that longitudinal sound velocity is roughly proportional to density. Shear velocities also increase with rock density [6].

Acoustic waves travel faster in stiff close-packed oxides such as MgO , Al_2O_3 , and Al_2MgO_4 , with longitudinal velocities near 10^6 cm/sec. More open structures like quartz, ice, and glass have velocities about half as large. Acoustic waves involve the transfer of impulse from atom to atom, and such a disturbance travels faster when atoms are in close contact, just as sound travels faster in a gas when it is pressurized. Thus there exists an inverse relation between acoustic velocity and volume per ion. PINNOW [7] has verified this conclusion by showing that the velocity to density ratio varies inversely with mean atomic mass, and that velocities can be predicted with an accuracy of better than 30% knowing the density and composition.

In addition to the dependence on volume, there is evidence that the velocity decreases with atomic mass. In the Column IV elements C, Si, Ge, Sn, and Pb, longitudinal velocities decrease from 1.8×10^6 for diamond to 0.2×10^6 cm/sec for lead. Force constants grow steadily smaller with atomic number because of the decrease in bond strength, resulting in smaller elastic constants and smaller acoustic velocities.

Volume compressibility and its reciprocal, the bulk modulus K , provide a convenient measure of the decrease in volume with pressure. Materials with large interatomic distances are generally more compressible than more tightly-bonded substances, hence the bulk modulus decreases with increasing atomic radius. The trends among metallic elements are illustrated in Fig. 71. Bulk modulus increases with valence, again because of stronger bonding, but the trends are less obvious as shown in the figure. ANDERSON and NAFE [9] plotted bulk modulus (reciprocal volume compressibility) against volume per ion pair demonstrating that most oxide data follow a similar relation. Bulk modulus is inversely proportional to volume, regardless of whether the volume change is caused by pressure, compositional variation, temperature, porosity, or phase changes. As might be expected, bulk modulus increases with density because short-range repulsive forces make it increasingly difficult to compress the solid as the atoms move closer together.

All materials compress under hydrostatic pressure, causing the volume to decrease as pressure increases. There is at least one material however, which *expands* in one direction. In elemental tellurium, the pitch of the spiral chains (Fig. 55) increases with pressure as adjacent chains move closer. This results in lengthening the chains along *c* while *a* and *b* grow smaller. Oriented tellurium films may prove useful in high-pressure equipment because of this unusual property.

Stiffness not only increases with the density of bonds, but with bonding strength as well. It is not surprising then, that stiffness can be correlated with hardness or with melting point, which also increases with

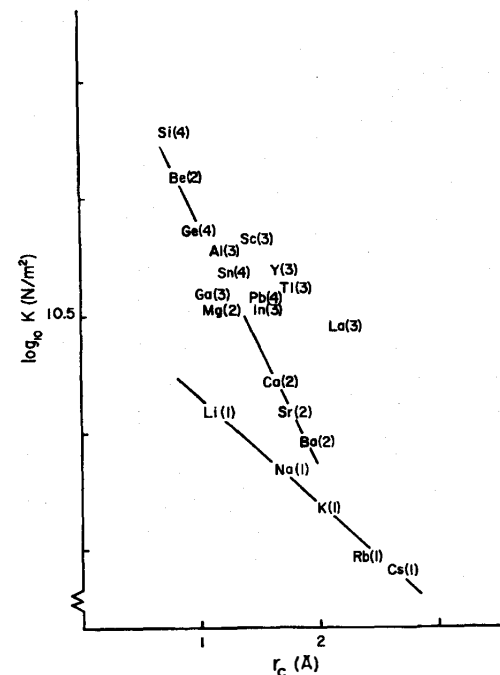


Fig. 71. Experimental values of bulk moduli K vs. Pauling radii r_c . The curves are computed by pseudo-potential methods and the experimental points are designated by the appropriate chemical symbols, the valencies being given in parentheses [8]

bond strength. Interatomic distances are a convenient measure of bond strength since crystallographic data are generally available [10]. Comparing compounds with the rock-salt structure shows that stiffness varies inversely with bond length (Fig. 72). The lithium halides are stiffer than the halides of the larger potassium and rubidium ions.

2. Mechanical Analog

In the lattice theory of elastic coefficients, stiffness coefficients are related to atomic force constants by determining the energy associated with various strain components. The calculation is cumbersome for a monatomic simple cubic lattice [11], and would be overwhelming for

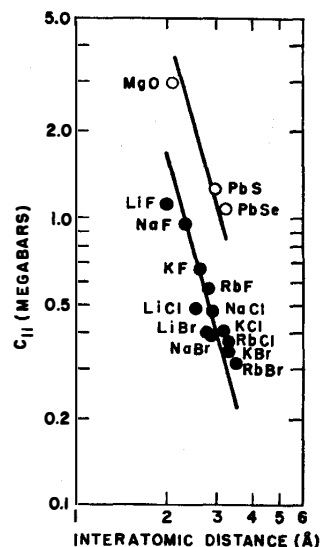


Fig. 72. Longitudinal stiffness coefficient c_{11} plotted as a function of near-neighbor distance for several rocksalt compounds. Univalent and divalent compounds are indicated by solid and open circles, respectively. The straight lines have slope -4

most oxide structures. To avoid mathematical complexity and gain further physical insight regarding the causes of elastic anisotropy, we make use of a simple mechanical analogy.

Atoms in a solid execute small oscillations of amplitude x about their equilibrium positions. If the potential energy is expanded in powers of x and all terms higher than quadratic are neglected, we have what is known as the harmonic approximation. The potential energy is represented by $(1/2)kx^2$ where k is the spring constant. Among the consequences of harmonic theory, however, is that elastic constants are independent of temperature and pressure, and thermal expansion is zero. Such effects arise from anharmonic (higher than quadratic) terms in the interatomic displacements. To provide an understanding of anharmonic effects, the dependence of spring constant on interatomic distance can be deduced from spectroscopic data, allowing one to estimate not only the elastic constants, but their temperature and pressure derivatives as well.

Tensile stiffness coefficients for most oxides are about 2 megabars (1 Mbar = 10^{12} dynes/cm²). Shearing coefficients are about 20% as large. Only in a few unusual materials such as paratellurite do shear waves

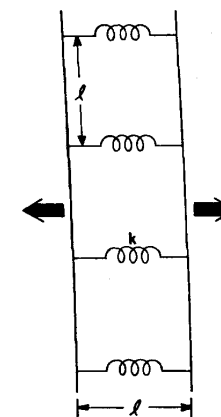


Fig. 73. A mechanical analog to an elastic crystal. Evenly-spaced identical springs with force constant k and length l are subjected to a tensile force F . The elastic stiffness coefficient is k/l

travel faster than longitudinal waves. The simple spring model shown in Fig. 73 provides some physical understanding of the magnitude and anisotropy of stiffness coefficients. A crystalline solid can be pictured as mass weights connected by springs. Let the length of the springs be l and the force constant k . If there are n/A springs per unit cross-sectional area, and all springs are identical, an applied force F is opposed by a restoring force,

$$F = \sigma A = nku = c A(u/l). \quad (1)$$

The spring displacement is u , giving rise to a strain u/l . Solving (1) for the stiffness coefficient gives $c = (n/A)kl$. Then n , l , and A can be evaluated from the crystal structure, but k cannot. Methods for determining force constants are discussed in the next paragraph. Typical values for k are 0.1–1.0 md/Å for bending force constants and 1–10 md/Å for stretching constants. Both types of deformation come into play in solids. When an SiO_4 tetrahedron is stressed, for instance, both stretching and bending will take place. Si–O force constants [12] are fairly typical with stretching constants 4–5 md/Å and bending constants 0.6–0.9 md/Å, while those involving Al are 10–20% smaller [13]. A careful analysis would be required to determine the correct force constant to use in (1), but in any case all the atomic force constants have not been determined from spectroscopic data. When an average value $k \sim 1$ md/Å is sub-

stituted 1), elastic stiffness coefficients of the right magnitude. Taking $l \sim 3 \text{ \AA}$, $\frac{n}{A} \sim 1/l^2 \sim 0.1 \text{ \AA}^{-2}$ gives $c \sim 3 \times 10^{12}$ comparable to the experimental value.

For constants can be estimated from first principles using potential functions. For an atom in its equilibrium position in potential energy determined by a balance of attractive and repulsive overlap forces. The potential energy is a function of x , the displacement from the equilibrium position. For small displacements, V is proportional to x^2 , and the restoring force is $F = -\frac{dV}{dx} = -kx$, where k is the force constant. Thus k is given by the second derivative, $k = d^2V/dx^2$, evaluated near $x = 0$.

Potential energy functions are known for only the simplest diatomic molecules, making it impractical to determine force constants in these cases. A more useful approach is to obtain k from infrared spectra. Quartz and several other minerals have absorption maxima in the same range [14]. These absorption peaks are caused by vibrations in which anions at adjacent sites move in opposite directions—the so-called stretching modes. Bending and rocking motions give rise to the lower-frequency infrared spectra.

Force constants computed for the various modes lead to values of k in the range 1 to 10 md/Å, as illustrated in the following calculation. Consider a hypothetical diatomic molecule which absorbs infrared radiation at a wavelength of 10μ , similar to the oxides. The molecule can be pictured as two atoms connected by a spring. Using the harmonic oscillator model, solving for the force constant k gives $m(2\pi c/\lambda)^2$, where λ is the wavelength, c the speed of light, and m the reduced mass. For m about 20 times the mass of a proton, resulting in a force constant of 2 md/Å.

Tables of force constants [15] derived from infrared spectra show that typical values are within an order of magnitude of 10⁵ dynes/cm (1 md/Å). Stretching force constants are plotted as a function of interatomic distance in Fig. 74. As might be expected, the force constant decreases with increasing bond length, though it is not surprising that so many different bond types fall along the same curve. In general the strongest bonds have the largest force constants. Deep potential wells have larger second derivatives when well bottoms are similar. Thus, for example, it is found that the stretching force constants for C—C, C=C, and C≡C are about 5, 10, and 16 md/Å, respectively. For bending motions, force constants lie in the range 0.1–1 md/Å. Bending force constants are much smaller than stretching force constants.

Tables of force constants [15] derived from infrared spectra show that typical values are within an order of magnitude of 10⁵ dynes/cm (1 md/Å). Stretching force constants are plotted as a function of interatomic distance in Fig. 74. As might be expected, the force constant decreases with increasing bond length, though it is not surprising that so many different bond types fall along the same curve. In general the strongest bonds have the largest force constants. Deep potential wells have larger second derivatives when well bottoms are similar. Thus, for example, it is found that the stretching force constants for C—C, C=C, and C≡C are about 5, 10, and 16 md/Å, respectively. For bending motions, force constants lie in the range 0.1–1 md/Å. Bending force constants are much smaller than stretching force constants.

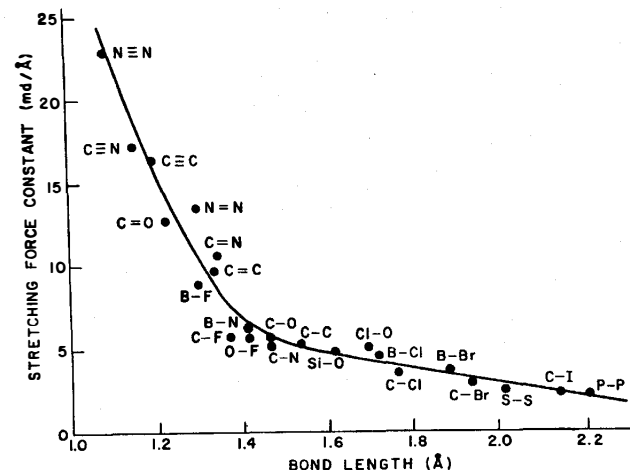


Fig. 74. Relationship between force constant and interatomic distance. Stretching force constants are from WILSON et al. [15], and interatomic distances from SUTTON [16].

because the repulsive overlap potential dominates when atoms move toward one another, increasing the force constant for stretching motion.

In crystals, shearing stiffnesses are about five times smaller than tensile stiffness. The difference can be attributed to the force constants since shearing generally involves bending motions whereas elongation involves the stretching of bonds. Force constants are larger for stretching, and elastic stiffness is proportional to the force constant.

Returning to the plot of stiffness against interatomic distance shown in Fig. 72, it is obvious that the c_{11} coefficients vary inversely with bond length. A straight line of slope -4 can be drawn through the alkali halide data, an observation that can be rationalized as follows [10]. The electrostatic potential energy for two charges q and q' separated by a distance l is $V = q'q/l$. As explained previously, the force constant is obtained from the second derivative of V , so that $k \propto 1/l^3$. Using the spring model, the elastic stiffness $c = k/l$, and is therefore proportional to $1/l^4$. Note that the data points for MgO, PbS, and the other divalent compounds lie above the alkali halide line. Electrostatic energy is approximately four times greater for these compounds because of the doubled charges. Force constants and stiffness coefficients will be four times greater also. When the measured stiffness values are corrected for valence, the points fall near the line for monovalent crystals.

The proportionality between stiffness and $1/l^4$ holds for glasses as well as crystals. Based on this relation, MAKASHIMA and MACKENZIE [17] have derived an equation for the direct calculation of Young's modulus of oxide glasses from their chemical compositions, obtaining excellent agreement for over thirty different glasses. Measured moduli range from about 0.2 Mbar for a lead borate glass to 1.5 Mbar for a glass containing nearly equal proportions of SiO_2 , Al_2O_3 , MgO , and BeO .

3. Elastic Anisotropy

The relationship between crystal structure and elastic properties can be illustrated with some of the simple structure types in the cubic system. In general, cubic crystals are not elastically isotropic [18]. The tensile stiffness relating stress to strain for an arbitrary direction in a cubic crystal is given by

$$c'_{11} = c_{11} - 2(c_{11} - c_{12} - 2c_{44})(a_1^2 a_2^2 + a_1^2 a_3^2 + a_2^2 a_3^2).$$

The equation involves the three independent stiffness coefficients (c_{11} , c_{12} , c_{44}) and the direction cosines (a_1 , a_2 , a_3) between the measurement direction and the three cube axes.

The anisotropy of c'_{11} can be discussed in terms of an anisotropy factor $A = 2c_{44}/(c_{11} - c_{12})$. If $A = 1$, $c'_{11} = c_{11}$ for all directions, and the crystal is elastically isotropic. If $A < 1$, the crystal is stiffest along the $\langle 100 \rangle$ cube edges, and most compliant along the $\langle 111 \rangle$ body diagonals. In the cubic system, there are, of course, three equivalent cube edges and four equivalent body diagonals. When $A > 1$, the crystal is compliant along $[100]$ and stiff along $[111]$. Stiffness coefficients for other directions are always intermediate between the values along $[100]$ and $[111]$. Measurements along $[110]$ are closer to the $[111]$ values than to $[100]$ because the angle between $[110]$ and $[111]$ is 10° smaller than between $[110]$ and $[100]$.

Elastic constants and anisotropy factors for a number of cubic materials are listed in Table 19. Note that anisotropy factors for similar materials tend to group together. The alkali metals Li, Na, and K have the largest A values, while RbI and other ionic crystals with the rocksalt structure have the smallest. Atomic bonding along several principal directions in these materials is illustrated in Fig. 75. In body-centered cubic metals the bonds to nearest-neighbor atoms are directed along the $[111]$ body diagonals; the bonds form uninterrupted chains in these directions. In the rocksalt structure, the bonds form uninterrupted chains along the $[100]$ cell edges.

Table 19. Elastic stiffness coefficients and anisotropy factors for a number of cubic crystals. Structure types included are body-centered cubic (BCC), face-centered cubic (FCC), diamond (D), rocksalt (RS), zincblende (ZB) and fluorite (F). (Data from CHUNG and BUESSEM [18])

Compound	Structure	c_{11}	c_{12}	c_{44}	A
Li	BCC	0.135	0.114	0.088	8.4
Na	BCC	0.074	0.062	0.042	7.2
K	BCC	0.037	0.031	0.019	6.7
Cu	FCC	1.68	1.21	0.76	3.2
Ag	FCC	1.24	0.94	0.46	3.0
Au	FCC	1.92	1.63	0.42	2.9
C	D	10.20	2.50	4.92	1.3
Si	D	1.66	0.64	0.80	1.6
Ge	D	1.30	0.49	0.67	1.7
LiF	RS	1.12	0.45	0.63	1.9
LiCl	RS	0.494	0.228	0.246	1.9
LiBr	RS	0.394	0.187	0.193	1.9
NaF	RS	0.970	0.244	0.281	0.77
NaCl	RS	0.485	0.125	0.127	0.71
NaBr	RS	0.397	0.106	0.099	0.68
KF	RS	0.656	0.146	0.125	0.49
KCl	RS	0.405	0.066	0.063	0.37
KBr	RS	0.346	0.056	0.052	0.36
RbF	RS	0.552	0.140	0.093	0.45
RbCl	RS	0.363	0.062	0.047	0.31
RbBr	RS	0.314	0.048	0.038	0.29
MgO	RS	2.96	0.95	1.56	1.55
PbS	RS	1.27	0.298	0.248	0.51
PbSe	RS	1.07	0.077	0.130	0.26
AlSb	ZB	0.89	0.44	0.42	1.8
InSb	ZB	0.83	0.45	0.40	2.1
GaSb	ZB	0.89	0.40	0.43	1.8
GaAs	ZB	1.19	0.60	0.59	2.0
ZnS	ZB	0.98	0.59	0.45	2.3
ZnSe	ZB	0.81	0.49	0.44	2.7
ZnTe	ZB	0.71	0.41	0.31	2.0
CdTe	ZB	0.54	0.37	0.20	2.4
CaF ₂	F	1.64	0.47	0.34	0.6
SrF ₂	F	1.24	0.43	0.31	0.8
BaF ₂	F	0.90	0.41	0.25	1.0
PbF ₂	F	0.89	0.49	0.25	1.2

Consider the effect of tensile stresses on these two structures. When BCC metals are stretched along $[111]$, the bonds parallel to this direction are lengthened, but no bending occurs. Thus the stiffness coefficient for the $[111]$ direction is expected to be large since only stretching force constants are involved. Compare this result with the case in

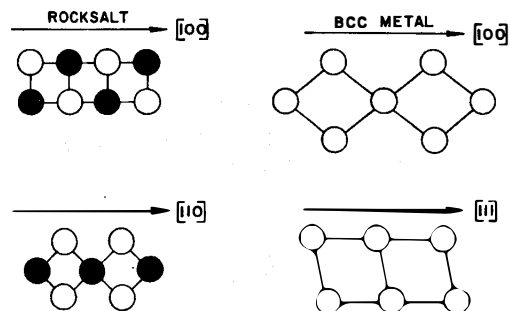


Fig. 75. Crystal structures of rocksalt and body-centered-cubic metals along several important directions. In NaCl the nearest neighbor bonds are in $\langle 100 \rangle$ directions. Rocksalt family crystals are generally stiffer in these directions. BCC metals are generally stiffer in $\langle 111 \rangle$ directions parallel to the bonds

which tensile stresses are applied along $[100]$. As shown in Fig. 75, the near-neighbor bonds in BCC metals follow a zig-zag path in the $[100]$ direction. When stretched along a cube edge, the bond will rotate as well as elongate. This results in a smaller stiffness coefficient than in the $[111]$ direction, since the force constants for bending motion are generally smaller than for stretching. The large anisotropy factors for alkali metals given in Table 19 can be rationalized in this way.

Anisotropy factors are generally smaller than one for alkali halides, which means the crystal is stiffest along cube edges. This is also the direction for near-neighbor bonds. Under tensile stress parallel to $[100]$, bonds elongate but do not rotate. Tensile stresses applied along $[110]$, $[111]$, and other directions lead to bending motions as well as elongation. Since bending is generally easier than stretching, the alkali halides are stiffest in the $[100]$ directions. As a result, the anisotropy factor A is usually less than 1. MgO and the lithium salts are exceptions for which $A > 1$. The reason is explained in Fig. 76 where sections of the MgO and KCl structures are illustrated with ionic radii drawn to scale. For rock-salt structures with small cations such as Li^+ and Mg^{2+} , the anions are in contact with one another. Bending motions become difficult when the anions are in contact. As a consequence, stiffness coefficients in the $[110]$ and $[111]$ directions become larger, and the anisotropy factor A increases for the Mg^{2+} and Li^+ salts. Bending is easier in KCl where the Cl^- anions are not in contact.

The importance of anion-anion forces has been pointed out by WEIDNER and SIMMONS [19]. In calculating the elastic properties of quartz and several alkali halides from a two-body central force model,

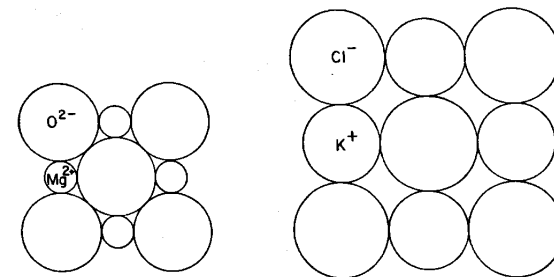


Fig. 76. KCl and MgO structures with the ionic radii drawn to scale. Anions are in contact in MgO, but not in KCl. Potassium chloride and most rocksalt structures are relatively compliant in $\langle 100 \rangle$ directions because bending can take place. Bending cannot take place in MgO and in lithium halides because the anions are in contact. Hence these crystals are stiffer in $\langle 110 \rangle$ directions

they found it necessary to include anion-anion interactions as well as cation-anion forces. Forces between anions are particularly important in determining compressibilities because overlap between ions occurs under pressure.

Other structure types follow a pattern similar to BCC and rocksalt crystals. The direction of bonding tends to be stiffer in most materials. In Cu, Ag, and other FCC metals the bonds are oriented along face diagonals. Face-centered cubic metals contain linear chains of near-neighbor bonds in all $[110]$ directions. We therefore expect higher stiffnesses in these directions. Since the $[110]$ direction is closer to $[111]$ than to $[100]$, anisotropy factors are expected to exceed unity. This agrees with the observed values listed in Table 19.

The situation is not as clear-cut in other simple structures because the bonds are not arranged in linear chains. In the diamond, zincblende, and fluorite structures, the bonds are oriented along $[111]$ directions but they are not continuously connected. Tensile strain along $[111]$ will therefore involve some bending as well as elongation. It is therefore reasonable that the anisotropy factors for these crystals are generally near 1, as expected for an isotropic material.

Most oxides are non-cubic with more complicated crystal structures than the materials just discussed. There are, nonetheless, certain regularities regarding c_{11} , c_{22} , and c_{33} , the tensile stiffness coefficients along the principal axes. The stiffness coefficients for silicate minerals presented in Table 20 show a correlation between elastic anisotropy and structure type [20]. All silicates contain (SiO_4) tetrahedra and, depending on how the tetrahedra are linked together, can be classified as framework, layer, chain or ring silicates.

Table 20. Longitudinal stiffness constants expressed in megabars [1]

Framework silicates		
α -quartz	SiO_2	$c_{11} = c_{22} = 0.9, c_{33} = 1.1$
silica glass	SiO_2	$c_{11} = c_{22} = c_{33} = 0.8$
Single chain silicates (pyroxenes)		
aegerine	$\text{NaFeSi}_2\text{O}_6$	$c_{11} = 1.9, c_{22} = 1.8, c_{33} = 2.3$
augite	$(\text{CaMgFe})\text{SiO}_3$	$c_{11} = 1.8, c_{22} = 1.5, c_{33} = 2.2$
diopside	$\text{CaMgSi}_2\text{O}_6$	$c_{11} = 2.0, c_{22} = 1.8, c_{33} = 2.4$
Double chain silicates (amphiboles)		
hornblende	$(\text{Ca, Na, K})_{2-3}(\text{Mg, Fe, Al})_5(\text{Si, Al})_8\text{O}_{22}(\text{OH})_2$	$c_{11} = 1.2, c_{22} = 1.8, c_{33} = 2.0$
Ring silicates		
beryl	$\text{Be}_3\text{Al}_2\text{Si}_6\text{O}_{18}$	$c_{11} = c_{22} = 3.1, c_{33} = 2.8$
tourmaline	$(\text{Na, Ca})(\text{Li, Mg, Al})_3(\text{Al, Fe, Mn})_6(\text{OH})_4(\text{BO}_3)_3\text{Si}_6\text{O}_{18}$	$c_{11} = c_{22} = 2.7, c_{33} = 1.6$
Layer silicates		
biotite	$\text{K}(\text{Mg, Fe})_3(\text{AlSi}_3\text{O}_{10})(\text{OH})_2$	$c_{11} = c_{22} = 1.9, c_{33} = 0.5$
muscovite	$\text{KAl}_2(\text{AlSi}_3\text{O}_{10})(\text{OH})_2$	$c_{11} = c_{22} = 1.8, c_{33} = 0.6$
phlogopite	$\text{KMg}_3(\text{AlSi}_3\text{O}_{10})(\text{OH})_2$	$c_{11} = c_{22} = 1.8, c_{33} = 0.5$

In framework silicates such as quartz and silica glass, the tetrahedra form three-dimensional networks. Since the bonding is nearly isotropic, there is no cleavage and little anisotropy in hardness or elasticity. Compare the longitudinal elastic moduli given in Table 20. When corrected for density ($\rho = 2.65$ gms/c.c. for quartz and 2.2 gms/c.c. for silica glass) the stiffness constants are nearly identical for the two forms of SiO_2 , substantiating the relation between bulk modulus and volume [9].

The influence of crystal structure becomes more obvious in the chain silicates. Pyroxenes contain SiO_3 single chains, and amphiboles Si_4O_{11} double chains as shown in Fig. 77. Elastic coefficients in Table 2 are referred to the measurement directions denoted by arrows in Fig. 77. Bonding is stronger along the chain direction giving rise to pronounced cleavage. We also expect the crystal to be stiffer in this direction, resulting in larger moduli. Experiment confirms this suggestion; the stiffness parallel to the chain (c_{33}) is the largest in pyroxenes and amphiboles. We also note that c_{22} has increased considerably in hornblende, possibly because of the increase of chain width in this direction.

Beryl and tourmaline, two ring silicates, show a similar correlation between stiffness and structure. Both contain Si_6O_{18} rings as illustrated schematically in Fig. 77. We expect strong bonding and greater stiffness

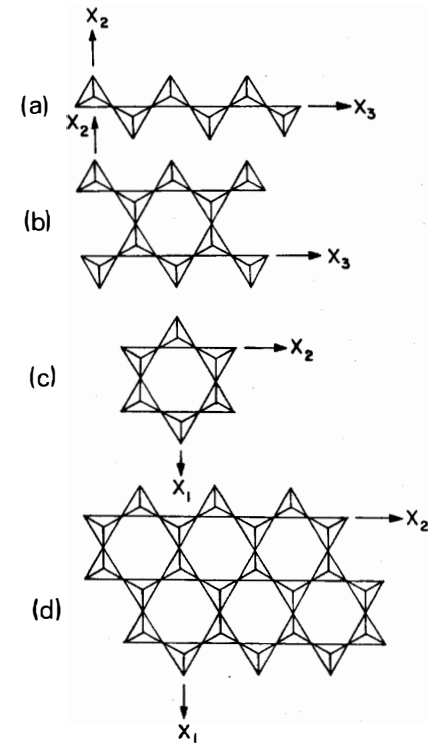


Fig. 77 a-d. Arrangements of SiO_4 tetrahedra in silicates: (a) Single chain silicates, (b) double chain silicates, (c) ring silicates, (d) layer silicates

in the plane of the ring, hence c_{33} should be smaller than c_{11} and c_{22} as observed. Beryl is not very anisotropic because of the strong Be-O and Al-O bonds connecting the rings.

When Si_6O_{18} rings adjoin one another, the tetrahedral layer found in micas is formed. The cleavage and stiffness anisotropy become very obvious in layer silicates, where c_{11} and c_{22} are three times larger than c_{33} . This is the maximum elastic anisotropy observed, for reasons that are explained later.

The mechanical analogy developed in the previous section can be applied to silicates. The analogy used to describe elastic anisotropy in minerals is one in which two mechanical springs represent atomic bonds with force constants k and K . To explain the elastic properties of solids containing both strong and weak bonds, consider the spring systems

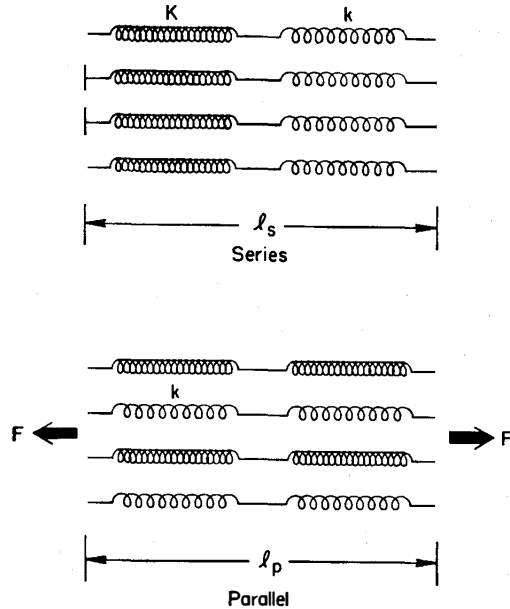


Fig. 78. Series and parallel connections of springs used to represent atomic bonds. Strong bonds have large force constants K , while weak bonds are easily stretched and have smaller constants k

illustrated in Fig. 78. When strong and weak springs are connected in series, most of the elastic energy is stored in the weak springs, while in the parallel connection the strong spring contains most of the energy. Let K and k be the force constants of two bonds arranged in series and parallel positions, as shown. This is a schematic representation of the bonding in mica. In muscovite Si-O and K-O bonds are in series for tensile stresses applied perpendicular to the sheet and in parallel when the applied forces lie in the plane. In pyroxenes, the parallel connection applies to measurements along the silicate chains, and series connections to the two perpendicular directions.

Analyzing the series arrangement for an applied tensile force F gives $F = \sigma A_s = n_s K u_K + n_s k u_k = c_s A_s u_s / l_s$ where σ is the stress acting on a surface of cross-sectional area A_s containing n_s chains, u_s / l_s is the resulting strain in the series (s) connection whose overall stiffness is c_s . The displacements of the springs are u_K and u_k with force constants K and k . An identical force applied to the parallel arrangement gives an analogous expression. $F = \sigma A_p = n_p K u_K + n_p k u_k = c_p A_p u_p / l_p$. For the series con-

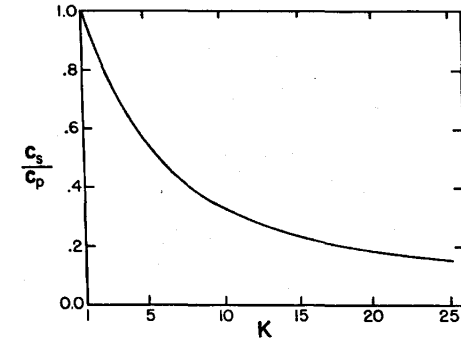


Fig. 79. Stiffness function of

connections plotted as a function of K/k . If k is far more pliant

than K , in the series connection both springs experience the same force so that their restoring forces are equal, $u_K K = u_k k$. The total displacement $u_s = u_k + u_K$, giving $u_k = u_s / (1 + k/K)$ and $u_K = u_s / (1 + K/k)$, and

$$c_s = \frac{n_s l_s}{A_s} \left(\frac{2 k K}{k + K} \right). \quad (3)$$

In solving the parallel chain system, it is obvious that the displacements of the different springs are equal and that $u_p = 2 u_k = 2 u_K$. Substitution in the force equation gives the elastic constant

$$c_p = \frac{n_p l_p}{A_p} \left(\frac{k + K}{2} \right). \quad (4)$$

Note that c_s and c_p are unequal, even when all the spring are identical ($k = K$). The elastic coefficients depend on bond lengths through l and on the number of chains per unit area in different directions.

To assess the effects of strong and weak bonding on the elastic constants, assume that the geometric factors are about equal so that $n_p l_p / A_p = n_s l_s / A_s$, giving the ratio $c_s / c_p = 4 k K / (k + K)^2$. In Fig. 79, the quantity c_s / c_p is plotted as a function of K/k to illustrate the effects of mixed bonding. When $K/k = 1$, all bonds have the same force constant, and the elastic constants are of course the same for series and parallel connection, so that $c_s / c_p = 1$. At the other extreme $c_s / c_p \rightarrow 0$ as $K/k \rightarrow \infty$ but the approach to zero is very slow. For $K/k = 2$, $c_s = 0.9 c_p$ and even for $K/k = 10$, $c_s = 0.3 c_p$. Since force constants for various chemical bonds

are all within an order of magnitude of one another, the expected maximum elastic anisotropy is about 3:1, as observed in muscovite (Table 20). In all cases $c_p > c_s$, as observed experimentally.

4. Pressure Dependence of the Elastic Stiffness

The pressure derivatives of the elastic coefficients of minerals determine changes in seismic wave velocities deep within the earth, and are strong indicators of the onset of phase transformation. Elastic stiffness coefficients and their initial pressure derivatives for four oxides are listed in Table 21.

Using the spring model just described, three observations are to be rationalized: 1. The pressure derivatives are all about one to ten megabars/megabar (dimensionless). 2. Large stiffnesses usually show greater pressure derivatives than small ones: if $c_{11} > c_{22}$, then $(\partial c_{11}/\partial P) > (\partial c_{22}/\partial P)$. 3. Pressure derivatives of the stiffnesses are positive in dense-packed structures but in open structures are occasionally negative. Quartz and beryl each have one negative derivative but the close-packed corundum and forsterite structures show none.

To estimate the pressure dependence of the elastic stiffness we again make the approximation that $n/A \sim 1/l^2$, then $c = (n/A)kl = k/l$, and $(dc/dP) = (1/l)(dk/dP) - (k/l^2)(dl/dP)$. Assuming an isotropic solid, $dP = -(dl)(c/l)$ so that

$$\frac{dc}{dP} = -\frac{1}{c} \frac{dk}{dl} + \frac{k}{lc}. \quad (5)$$

Table 21. Comparison of elastic stiffness and their initial pressure derivatives for four oxides. Adiabatic stiffness c_{ij} are expressed in megabars, and the pressure derivatives $\partial c_{ij}/\partial P$ are dimensionless

ij	Beryl [21]		Quartz [22]		Corundum [23]		Forsterite [24]	
	c_{ij}	$\partial c_{ij}/\partial P$	c_{ij}	$\partial c_{ij}/\partial P$	c_{ij}	$\partial c_{ij}/\partial P$	c_{ij}	$\partial c_{ij}/\partial P$
11	3.09	4.5	0.87	3.3	4.98	6.2	3.29	8.3
22	3.09	4.5	0.87	3.3	4.98	6.2	2.01	5.9
33	2.83	3.4	1.06	10.8	5.02	5.0	2.36	6.2
44	0.66	-0.2	0.58	2.7	1.47	2.2	0.67	2.1
55	0.66	-0.2	0.58	2.7	1.47	2.2	0.81	1.7
66	0.90	0.3	0.40	-2.7	1.68	1.5	0.81	2.3
12	1.29	3.9	0.07	8.7	1.63	3.3	0.07	4.3
13	1.19	3.3	0.12	6.0	1.17	3.7	0.07	4.2
23	1.19	3.3	0.12	6.0	1.17	3.7	0.07	3.5
14	0	0	-0.18	1.9	-0.23	0.1	0	0

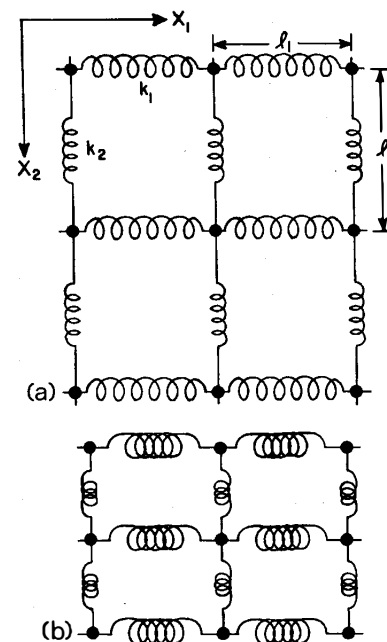


Fig. 80a and b. Anisotropic spring model illustrating the pressure dependence of elastic coefficients. Low-pressure (a) and high-pressure (b) configurations are shown

A rough value for dk/dl can be obtained by examining how k varies with interatomic distance. Short strong bonds have larger stiffnesses than long bonds. The bond stiffness for Si-O is about 10% larger than that for Al-O, and the bond length is about 10% shorter. Therefore dk/dl is roughly $-2 \text{ md}/\text{\AA}^2$. Substituting this value in (5) along with $c = 3 \times 10^{12} \text{ dyne/cm}^2$, $k = 1 \text{ md}/\text{\AA}$ and $l = 3 \text{ \AA}$ gives $dc/dP \sim -5$ (dimensionless), the right order of magnitude.

To explain the second observation consider the anisotropic structure in Fig. 80. The structure contains tightly bonded atoms in the X_1 direction and very loose bonding along X_2 . From arguments previously presented $c_{11} > c_{22}$. Now consider their pressure derivatives. From Eq. (1) the change in stiffness with pressure is related to the change in the number of chains per unit area n/A , their repeat distance l , and bond stiffness k :

$$\frac{dc}{dP} = lk \frac{d(n/A)}{dP} + \frac{nk}{A} \frac{dl}{dP} + \frac{nl}{A} \frac{dk}{dP}. \quad (6)$$

Under pressure the structure will compress mainly along X_2 because of the weak bonding in that direction, giving the exaggerated deformation in Fig. 80.

For the X_1 direction there will be little change in l_1 and k_1 so that $(dc_{11}/dP) \sim l_1 k_1 d(n/A)/dP$. The number of chains per unit area increases rapidly with pressure because of the big reduction in l_2 , decreasing A and increasing n/A . Therefore c_{11} increases rapidly with pressure.

For direction X_2 , there is little change in n/A with pressure because l_1 hardly changes. Therefore $dc_{22}/dP \approx (n/A) [k_2(dl_2/dP) + l_2(dk_2/dP)]$. The length and spring constant are inversely related to one another so that the increase in spring constant is partially offset by change in length. Hence c_{22} will not increase rapidly with pressure.

The third observation regarding the pressure dependence is the occurrence of negative derivatives in open structures like beryl and quartz. When a close-packed structure is compressed, the atoms move closer together but this need not be true in an open structure where rotations can take place. To determine the effect on the elastic constants, consider Eq. (6) describing the pressure dependence of the stiffness. The new feature here is the pressure dependence of the stiffness k . If we are considering the stiffness along X_1 , for example, k_1 may decrease with P because at high pressure a stress along X_1 produces a bending rather than a stretching motion. The stiffness coefficients for bending are considerably smaller than for stretching. Thus rotation can lead to negative pressure dependence of shearing stiffness coefficients.

5. Temperature Dependence of the Elastic Stiffness

Most materials soften as they become warmer so that elastic stiffness decreases as temperature increases. Some representative values of dc/dT for oxides are given in Table 22. The fractional change in stiffness $(1/c)(dc/dT)$ is of the order -2×10^{-4} per $^\circ\text{C}$. The variation of the elastic coefficients with temperature is of some geophysical interest because of the increase in temperature with depth. Stiffness increases with pressure so that acoustic waves increase speed with depth, but the increase is partly offset by the temperature effect. The temperature dependence of the elastic constants is also important in acoustic delay lines and in piezoelectric oscillators and filters. Variations of the delay time or resonant frequencies are undesirable in these devices.

The mechanical spring model just discussed also provides an explanation of the temperature dependence of the elastic stiffness. To estimate the size of dc/dT , we assume an isotropic model of identical

Table 22. Temperature coefficients of elastic stiffness for several oxides [1]. $T_c = (1/c)(dc/dT)$ and is expressed in units of 10^{-4} per $^\circ\text{C}$

springs, for w
constant of the

ly. The force
re derivative is

$$\frac{dc}{dT} = \frac{d}{dT} \left(\frac{k}{l} \right) = \frac{1}{l} \frac{dk}{dT} - \frac{k}{l^2} \frac{dl}{dT}. \quad (7)$$

The second term is directly proportional to the linear thermal expansion coefficient $\alpha = (1/l)(dl/dT)$. The first term depends on the change in force constant with temperature. Chemical bonds grow weaker with increasing length and the force constant becomes smaller. If we assume that the change in k depends primarily on l , then $(dk/dT) \approx (dk/dl)(dl/dT)$, and the variation stiffness with temperature becomes:

$$\frac{dc}{dT} = \alpha \frac{dk}{dl} - \frac{k}{l} \alpha. \quad (8)$$

As shown in the previous section, $dk/dl \sim -2 \text{ md}/\text{\AA}^2$, $k \sim 1 \text{ md}/\text{\AA}$, $l \sim 3 \text{\AA}$, and $c \sim 3 \times 10^{12} \text{ dynes/cm}^2$. Thermal expansion coefficients for oxides are about 10^{-5} per $^\circ\text{C}$.

Substituting these values gives a fractional change $(1/c)(dc/dT) \sim 10^{-4}/^\circ\text{C}$, which is the right order of magnitude. This value is small, but is several times larger than the thermal expansion coefficient α . This is important because the thermal expansion coefficients are crucial in delay line and frequency-standard devices. Thus in searching for zero-temperature coefficients, materials with unusual elastic properties are needed. In particular, it is important to find materials with *positive* temperature coefficients $(1/c)(dc/dT)$. In the next section we consider the circumstances under which this might occur.

6. Temperature-Compensated Materials

New temperature-compensated piezoelectric crystals are needed for acoustic surface-wave matched filters, encoders, decoders, and related signal processing devices [25]. The requirements are similar to but not

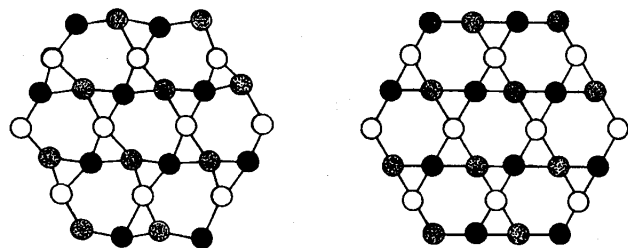


Fig. 81
decrea:
expans

identical with those for frequency control standards. Temperature stability is important in both cases, but large piezoelectric-coupling factors are also essential for surface-wave devices because of high losses. This is the principal disadvantage for quartz, which has a number of temperature-compensated orientations, but relatively small electro-mechanical coupling parameters near 0.1.

Materials with unusual values of T_c are therefore of special interest for temperature-compensated devices. Quartz is such a material since T_c for shear about the z-axis is positive (Table 22). The structures of α - and β -quartz (Fig. 81) provide an understanding of this behavior. The α -quartz structure is a partially collapsed derivative of β -quartz. At higher temperatures the SiO_4 tetrahedra rotate to an open, fully-expanded structure, undergoing a displacive phase transition at 573°C to the β -quartz structure. Quartz shows a rather high rate of thermal expansion at room temperature due to the rotation of the tetrahedra.

In many ways, the crystallochemical factors governing thermal expansion [26, 27] coefficients are similar to those which are important for elastic properties. Strong interatomic forces are associated with low thermal expansion and low elastic compliance, weak forces with high compliance. Moreover, the thermal expansion coefficient can also be attributed to bond-length changes and to tilting changes, like the stiffness coefficient. Materials with unusual thermal expansion coefficients generally show rotational motions in the crystal structure.

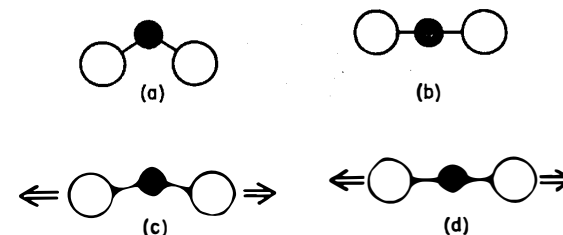


Fig. 82a-d. Models indicating the origin of positive T_c coefficients in open crystal structures. (a) Shows three atoms connected by bent bonds. At higher temperatures (b) the bond straightens. When stressed, the bent bonds both lengthen and rotate, as shown in (c). When the straight bonds are stressed, only lengthening takes place (d). (c) Shows larger overall change in length than (d), hence the low-temperature structure is more compliant

Thermal expansion coefficients of quartz become even larger just below the transformation temperature and then decrease abruptly to near zero when the fully-expanded structure is achieved. Quantitative calculations show that the thermal expansion is due chiefly to tetrahedral rotations, with only a minor contribution from thermal motion [28]. The anomalous value of T_{c66} is related to the rotation effect. The coefficient c_{66} relates a shearing stress about the z-axis to a shearing strain about the same axis—the same type of motion involved in the rotation of tetrahedra in transforming from α - to β -quartz. At room temperature the Si-O-Si bonds are quite bent, but they straighten with increasing temperature as the structure grows closer to β -quartz. Consider the effect of mechanical stress on such arrangements. When bent bonds are stretched, the bonds rotate as well as deform (Fig. 82), resulting in a sizeable strain. Thus the stiffness is rather small at room temperature. When the straightened high-temperature structure is stressed, only deformation occurs since the structure does not permit rotation. As a result, there is less strain and the stiffness increases with temperature. A positive value of T_c can be related to rotational effects in this way.

In the previous section, the temperature coefficient of the elastic stiffness c was described in terms of a mechanical spring model. There it was shown that $T_c = (1/c)(dc/dT) = (1/lc)(dk/dT) - (k/l^2c)(dl/dT)$. In this equation, l is the length of the spring and k is the spring constant. For most materials, T_c is determined by the first term on the right, resulting from the change in spring constant with temperature. The second term arises from thermal expansion, and is generally smaller. The spring constant usually decreases with temperature because of thermal vibrations, so that dk/dT is usually negative and so is T_c .

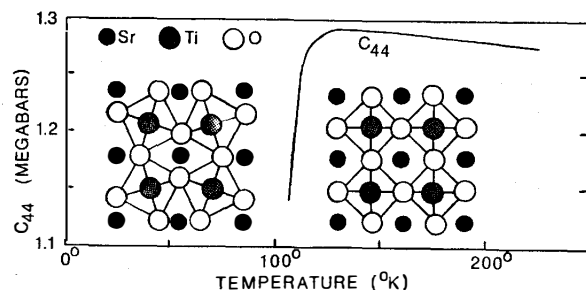


Fig. 83. Temperature dependence of c_{44} in SrTiO_3 . High- and low-temperature crystal structures illustrate the rotations which occur at the 110 °K transition

This need not be so when rotations occur because rotational spring constants are smaller than stretching spring constants. For Si–O bonds, the stretching constant is about 5 md/Å while bending spring constants are less than 1 md/Å. In kinked bonds, both stretching and bending occurs under stress. The effective force constant is smaller than in the high-temperature case where only stretching takes place. In this situation dk/dT is positive, as is T_c , because the force constant changes character with increasing temperature.

In searching for new materials with positive temperature coefficients, we look to open structures in which sizeable rotations can occur. Coordination numbers are usually small in open structures, so that oxygens are bonded to only 1, 2, or 3 neighbors. In framework aluminosilicates such as the feldspars and zeolites, the oxygen forms two strong bonds to Si^{4+} or Al^{3+} . Leucite, albite, cristobalite, and other minerals show puckering transitions [29] similar to quartz, and can be expected to show unusual elastic constants. Phase transitions are a second clue to the occurrence of positive T_c values, since rotations sometimes lead to a change in structure.

Close-packed structures are generally not conducive to rotational movements, although there are exceptions to this. SrTiO_3 shows a beautiful rotational transition near 110 °K which is accomplished by anomalous elastic behavior. At room temperature strontium titanate has the ideal cubic perovskite structure (Fig. 83) with TiO_6 octahedra connected in straight chains. Temperature coefficients of the elastic constants are quite normal (Table 22). Below 150 °K, however, the shear coefficient c_{44} drops rapidly, giving a large positive temperature coefficient [30]. Neutron scattering experiments [31] show that the TiO_6 octahedra are undergoing large thermal oscillations in this temperature range, the so-called soft-mode behavior. The symmetry changes from

cubic to tetragonal at the 110 °K phase transition as the soft mode condenses to form a distorted perovskite (Fig. 83). Alternate octahedra rotate clockwise and counterclockwise, producing kinked Ti–O–Ti chains in the low-temperature structure.

7. Surface Wave Materials

A new technology based on elastic surface waves has led to the development of compact and inexpensive signal-processing components. Surface waves are used in delay lines, filters, and more sophisticated devices. The size and weight savings can be as much as 10^5 , the ratio of the velocity of light to the speed of sound. For instance, an acoustic path of 1 cm delays the signal several microseconds—equivalent to a kilometer of coaxial cable or waveguide. Surface waves are always accessible for signal processing, a clear advantage over bulk waves. In the 1 GHz range, surface wave wavelengths are a few microns, making microcircuits a real possibility. The waves can be focused, channeled, sensed, mixed, and are compatible with integrated circuit technology.

Rayleigh waves traveling on the surface of a crystalline solid cause a point on the surface to describe a rotating ellipse with both vertical and horizontal amplitude, like a ripple on a pond. Most of the energy is confined to a surfacelayer one wavelength thick. Increasing the frequency increases the power density giving larger signals.

In a Rayleigh surface-wave device, an interdigital transducer converts an electromagnetic signal to an elastic surface wave. Displacement amplitudes for Rayleigh waves decrease exponentially with depth and are confined to within one acoustic wavelength of the surface. At 10^3 MHz the acoustic wavelength is about 4 μ . An interdigital transducer consists of a thin-film metal grating with half-wavelength spacing deposited on a piezoelectric substrate. Electrode patterns are produced with the same photo-lithographic processes used for planar integrated circuits. A voltage pulse applied to the grating produces a localized mechanical strain which propagates along the surface.

Materials with high piezoelectric coupling are needed to gain low insertion loss and wide bandwidth. Lithium niobate, lithium tantalate and bismuth germanium oxide have larger piezoelectric constants than quartz, but zero-temperature coefficient cuts are required for signal processing. A positive temperature coefficient for at least one elastic stiffness constant is needed for temperature compensation. Only quartz and tellurium dioxide have thus far yielded compensated cuts for surface wave applications and neither is strongly piezoelectric.

Pure Rayleigh waves are non-dispersive, traveling with the same velocity at all frequencies. This is an advantage in reducing signal distortion, but filters and pulse compression delay lines require dispersion. Dispersion can be controlled by depositing a surface layer on a substrate. At low frequencies, the Rayleigh wave penetrates deep into the bulk so that the velocity is determined by the substrate, while at higher frequencies the wave moves closer to the surface until it is concentrated within the surface layer. Thus the velocity changes smoothly from that of the substrate to that of the surface. Depositing a stiff deposit on a soft substrate gives a "fast on slow" combination. A mechanically soft deposit will reverse the dispersion characteristic. Silicon deposited on a sapphire substrate has been used in many experiments. Dispersion can be altered from point to point by tailoring the surface deposit in thickness and composition.

In choosing a substrate material for surface-wave filters, it is important to maximize the coupling between the electric field produced by the transducer substrate and the acoustic surface wave. The coupling coefficient depends on propagation direction as well as the nature of the piezoelectric substrate. Single crystal substrates are preferable to piezoelectric ceramics because their uniformity and freedom from aging effects. Most piezoelectric ceramics are slightly porous, making it difficult to deposit miniature electrode patterns. The surface must be suitable for photolithography.

The dielectric constant of the substrate determines the impedance of the device; it is important to have a low dielectric constant to maintain a reasonably high impedance. For narrow-band filters, the variation of wave velocity with temperature must be eliminated. This can sometimes be accomplished by orienting the substrate properly. In anisotropic materials, it is generally more convenient to work with directions in which the energy flow is perpendicular to the wave front.

8. Molecular Geometry and Molecular Flexibility

Some plastics are rigid and others are flexible. The influence of chemical structure on molecular flexibility can be illustrated with the linear polymers polyethylene and polyisobutylene [32]. Polyethylene is a hard crystalline plastic, while polyisobutylene is an amorphous, soft rubbery material which gives crystalline X-ray diffraction patterns only when stretched.

For a linear polymer to fit into a regular crystal structure, the chain itself must assume an arrangement which makes this possible. For polyethylene, such an arrangement is not only possible, but is thermo-

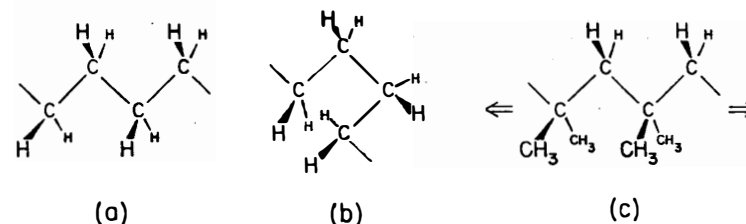


Fig. 84 a-c. The extended (a) and bent (b) configurations of polyethylene, a relatively rigid crystalline plastic. The extended configuration of rubber-like polyisobutylene shown in (c) is stable only under stress

dynamically preferred. Structure analysis of polyethylene has shown that the chains are in the extended or linear arrangement (Fig. 84). In this form the chains are readily packed together in a regular array necessary for crystallinity. In the liquid state, polyethylene contains a number of bent bonds as well.

The extended conformation of polyisobutylene is also shown in Fig. 84. Alternate carbons in the backbone are bonded to methyl groups rather than hydrogens as in polyethylene. The distance between alternate carbons is 2.54 Å. With hydrogens as side groups, the sum of van der Waals radii is 2.4 Å, allowing sufficient room, and explaining why the extended conformation is stable in polyethylene. However, the sum of van der Waals radii for neighboring methyl groups is about 4.0 Å, much larger than the distance between carbons in the extended position. Therefore the extended form is unstable in polyisobutylene because of steric compression and the molecule prefers a randomly coiled conformation which cannot fit into a periodic crystalline array.

When polyisobutylene is stretched, the chains are extended in the stress direction. They cannot become fully extended as in polyethylene, but assume a nearly extended conformation in which neighboring methyl groups are staggered to minimize repulsion. Thus each unit is twisted with respect to its neighbors and the methyl groups in polyisobutylene form a helix around the axis of the stressed polymer molecule. As soon as tension is released polyisobutylene returns to its original unstressed length and its randomized coiled geometry. At room temperature the inflexible crystalline state is stable only under stress.

Inorganic chain structures sometimes show thermal transitions resembling those in organic polymers, forming glasses at low temperatures and becoming rubbery above a glass-transition temperature before melting. An advantage of inorganic polymers over their organic counterparts is their resistance to oxidation and chemical degradation.

The silicate chains in glass and crystalline minerals are too strongly cross-linked to be flexible. Instead of rubbery elastomeric behavior, silicates are generally brittle with high melting points. Basically the need is for an inorganic polymer with linear chains and non-ionic substituent groups to confer flexibility over a wide temperature range. Covalently-bonded backbones can be devised from elements such as B, Si, Ge, Sn, N, P, As, Sb, O, S, Se, and Te.

One of the first inorganic polymers was sulfur. Quenching molten sulfur in water gives a rubbery high-polymer form which reverts slowly to the crystalline form containing S_8 rings. Silicone polymers are more practical than sulfur. Polydimethylsiloxane the most widely used silicone consists of a $-\text{Si}-\text{O}-\text{Si}-\text{O}-$ backbone with two CH_3 groups attached to each silicon. Comparing the silicone with a pyroxene chain silicate, the methyl groups replace the two side oxygen ions of each SiO_4 tetrahedra, leaving the central chain unbroken. Silicones are prepared from a cyclic ring compound, octamethylcyclotetrasiloxane. Polymers containing as many as 30000 $-\text{Si}-\text{O}-$ units are obtained on heating the ring compound above 100°C in the presence of an acid or base. Silicone rubber is made from the polymer by crosslinking the chains to prevent slipping past one another. The temperature range of silicone rubber is -60 to 250°C , one of the most flexible molecules known. The high flexibility has been attributed to the lack of electric charge on the side groups, and to the fact that side groups are attached to alternate backbone atoms, resulting in less steric hindrance between side groups during bending. Silicones are also useful as surface coatings and biomedical applications because they repel water.

Siloxane chains break down to form rings above 250°C . Double chain siloxane ladder compounds are more stable but less flexible. Polydichlorophosphazene $(\text{NPCl}_2)_n$ is another remarkable elastomer with mechanical properties superior to natural rubber.

The development of inorganic polymers is still in its infancy with many more elements and hundreds of combinations yet to be explored [33].

9. Hardness

In 1822 the Austrian mineralogist Mohs proposed a hardness scale that has continued in use for the past 150 years: 1. talc $\text{Mg}_3\text{Si}_4\text{O}_{10}(\text{OH})_2$, 2. gypsum $\text{CaSO}_4 \cdot 2\text{H}_2\text{O}$, 3. calcite CaCO_3 , 4. fluorite CaF_2 , 5. apatite $\text{Ca}_5(\text{PO}_4)_3\text{F}$, 6. orthoclase KAlSi_3O_8 , 7. quartz SiO_2 , 8. topaz $\text{Al}_2\text{SiO}_4\text{F}_2$, 9. corundum Al_2O_3 , 10. diamond C. Hardness is defined as resistance to scratching, with the softer minerals being scratched by those higher in the scale. Relative hardness is a useful diagnostic property in

mineralogy, and is of great engineering importance, although the tests are empirical in nature. Indentation measurements (Brinell or Vickers) are somewhat more quantitative than scratch tests.

Strength of bonding is closely related to hardness. Van der Waals solids are very soft. In talc, the magnesium silicate layers are strongly bonded in two-dimensions, but there are no strong covalent, ionic, or even hydrogen-bonds between layers. Hence talc is much softer than other silicates.

Molecular solids are invariably soft with Mohs hardness rarely exceeding 3. The same is true of hydrogen bonded solids. Only in crystals such as glycine or lactose with an unusually large number of hydrogen bonds does the hardness exceed 3 [34]. In a hydrated salt, hardness decreases with increasing water content: anhydrite (CaSO_4) is harder than gypsum ($\text{CaSO}_4 \cdot 2\text{H}_2\text{O}$) and kieserite ($\text{MgSO}_4 \cdot \text{H}_2\text{O}$) is harder than epsomite ($\text{MgSO}_4 \cdot 7\text{H}_2\text{O}$).

Ionic crystals are harder than molecular crystals but softer than solids with three-dimensional covalent bonding, such as diamond and SiC. Ionic solids show a symbiotic variation between lattice energy and hardness, so that hardness is greater for increasing charge and decreasing ionic radius in a homologous series of salts [35].

In relation to crystallochemical parameters, hardness increases with packing density and valency, and decreases with ionic size. The correlations with ionic size and valence can be illustrated with isostructural compounds with the calcite structure. Magnesite (MgCO_3) has a hardness of $4\frac{1}{2}$ on Mohs scale, compared to only 3 for calcite (CaCO_3), showing how hardness decreases with increasing ionic radius. The radii of Mg^{2+} and Ca^{2+} are 0.72 and 1.00 Å, respectively. Soda niter (NaNO_3) also has the calcite structure, and the radii of Na^+ (1.02 Å) and Ca^{2+} are almost identical, yet sodium nitrate is softer (2) than calcite because of the decrease in valence. The strength of the ionic bonds in these materials determines the hardness since the ionic bonds are weaker than the covalent bonds in the carbonate and nitrate groups. The bond strength and hardness are directly proportional to valence and inversely proportional to interatomic distance.

Hardness increases with packing density. Comparing polymorphs, argonite is denser and harder than calcite, and quartz is both harder and denser than tridymite. Other factors being equal, hardness is determined by the number of bonds per unit volume. Framework silicates vary in hardness from 4 or 5 for zeolites, 6 for feldspars to 7 for quartz. The densities increase in the same order, 2.2 for zeolites, 2.56 for orthoclase and 2.65 g/c.c. for quartz. Silica glass has a hardness of 5 and a density of 2.3.

Metals do not appear on Mohs scale, but range from less than 1 to 7. Hardness increases with valence: alkali metals are extremely soft (~ 0.5),

alkaline earths about 2, aluminum 2.5, and transition metals 4–7. Copper, lead and other post-transition metals have low hardnesses (1–3). In general, the hardness of metals covers about the same range as ionic crystals, showing that the bonds are comparable in strength.

Carbides, borides and nitrides possess strong covalent bonds and great hardness. Cubic boron nitride (BN), boron carbide (B_4C), and silicon carbide (SiC) are excellent abrasives with hardnesses exceeding alumina. The addition of carbon to iron greatly increases hardness.

Anisotropic materials such as graphite or molybdenite often have high melting points but low hardness, seemingly violating the proportionality between hardness and lattice energy. The reason is that mechanical properties such as hardness and cleavage depend on the *weakest* bonds while melting and chemical reactivity depend on the *strongest* bonds.

Hardness decreases with increasing temperature, with soft materials showing a decrease of about 1 in hardness for a 20–100° temperature rise.

10. Grinding and Polishing

Anisotropy in hardness is important in determining grinding or lapping rates. These properties are technically important but are not easy to define quantitatively for grinding rates depend on the speed of lapping, the nature of the abrasive and on the forces involved. Nevertheless it is possible to discuss the relative grinding rates of various crystal faces and to give a qualitative explanation of their magnitudes in terms of crystal chemistry.

The grinding rates for diamond (Table 23) are of great interest to lapidary workers because certain faces can be polished much more rapidly than others. Not only is the face important but the direction of motion as well. The comparative lapping rates can be correlated with surface roughness with rougher surfaces producing greater friction and faster grinding rates [36]. The (111), (110), and (100) surfaces of diamond shown in Fig. 85 are not equally smooth.

Table 23. Relative grinding times required to remove a given thickness from a diamond crystal by polishing on various planes in several directions [36]

Plane	Direction	Time
(111)	any	$> 10^3$
(100)	$[0\bar{1}0]$	3
(100)	$[011]$	22
(110)	$[001]$	1
(110)	$[\bar{1}10]$	51

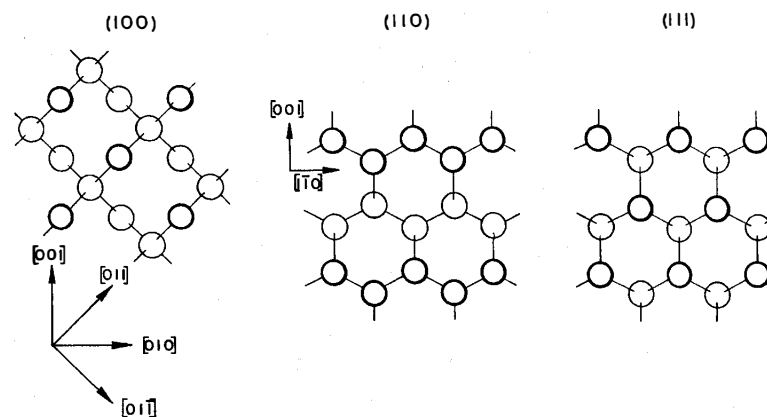


Fig. 85. Three principal surfaces of diamond with grinding directions indicated. Carbon atoms on upper surface are heavy circles and lower levels are lighter

The octahedral (111) faces of diamond are exceedingly difficult to polish. The surface is smooth and strongly bonded with each surface atom held in place with three bonds. Referring to Fig. 85, it can be seen that the (110) face has grooves parallel to $[\bar{1}10]$, the slow-grinding direction in this plane. Polishing proceeds much more rapidly in the perpendicular $[001]$ direction because of greater surface roughness when traversing the crystal perpendicular to the grooves. Motion in the $[010]$ and $[001]$ directions give the fastest polishing rates for the (100) face. There is always surface roughness in this direction which is at 45° to the grooves parallel to $[011]$ or $[0\bar{1}1]$.

Since Si and Ge are isostructural with diamond, crystal orientation is important in semiconductor processing [37]. Scribing is more difficult on the strongly bonded (111) plane than on (100), and etching rates vary also. For example, vapor etch rates for oriented Si slices in 5% HCl at 1200° C in H_2 are about twice as fast for (110) and (100) as for (111). For other etchants the ratio can be made as large as 50:1, a technique used to develop isolation moats. Epitaxial deposition rates for silicon are also orientation-dependent.

Webster's dictionary defines *polishing* as "to make smooth and glossy, usually by friction". Friction has two effects on the surface, abrasion and heating. The abrasive theory of polishing was described long ago by Newton in his treatise on "Opticks" written in 1668.

"In polishing glass with sand, putty (stannic oxide) or tripoli (diatomaceous earth composed mainly of silica) it is not to be imagined that

these substances can, by grating and fretting the glass, bring all its least particles to an accurate polish; so that all their surfaces shall be truly plain or truly spherical, and look all the same way, so together compose one even surface. The smaller the particles of these substances are, the smaller will be the scratches by which they continually fret and wear away the glass till it be polished; but be they never so small, they can wear away the glass no otherwise than by grating and scratching it, and breaking the protruberances; and therefore polish it no otherwise, than by bringing its roughness to a very fine grain, so that the scratches and frettings of the surface become too small to be visible."

The abrasion theory of polishing was an embarrassment to Newton because he found it difficult to reconcile specular reflection with the corpuscular theory of light. Corpuscles are diffusely scattered by even the smallest irregularities on the abraded surface. The wave theory of light removes the inconsistency. Any protruberances appreciably smaller than a wavelength are invisible, so that perfect reflection results.

Newton's superfine grinding theory went unchallenged until 1901 when Lord Rayleigh, another great English physicist, studied the behavior of surface scratches. When a scratched surface is polished smooth and then etched, the same scratches reappear. Sir George Beilby developed the melting theory of polishing to explain these observations. Frictional heating raises the temperature of protruberances on the surface. The localized heating causes melting, and molten material flows from peaks to valleys, filling them. In the abrasive theory, hills are worn away, while in the melting theory, the hills melt and flow, filling the valleys. In either case, a smooth polished surface results.

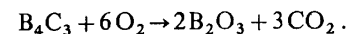
Bowden and Hughes attempted to resolve the question by performing polishing experiments on a number of different materials. They reasoned that if the abrasion theory is correct, then hard materials should polish softer substances. On the other hand, if melting occurs, the material with the lowest melting point is polished. After testing many materials, Bowden and Hughes found that the abrasive theory works best for materials with high melting points. Low melting metals obey the melting theory, forming a molten layer which resolidifies, forming a smooth polished surface.

The nature of the re-solidified surface, the Beilby layer, was subsequently investigated by G.I. Finch. Using low-energy electron diffraction, Finch found that diamond polishes differently than other gemstones. Diamond abrades on polishing while the others melt, consistent with their lower melting points. The melting point of carbon (4300°C) is twice that of other gems. The diffraction experiments revealed a thin Beilby layer on polished quartz and corundum. On cooling, the layer quickly recrystallizes in conformity with the under-

lying structure. For zircon and spinel the Beilby layer remains amorphous on all surfaces.

More recent experiments by RABINOWICZ [38] favor a size-effect theory. Abrasion dominates for rough grinding where large particles are broken off, but small particles are not as stable because of the large surface to volume ratio. Under fine grinding, a Beilby layer forms and polishing results.

Chemical reactions sometimes play a role in polishing. Alumina (Al_2O_3) polishes boron carbide (B_4C_3) despite its greater hardness and higher melting point. Alumina particles heat the boron carbide surface, oxidizing it.



Alumina then abrades the B_2O_3 surface layer, polishing boron carbide.

11. Friction and Wear

Hard ceramics, cemented-carbides, and cermets show excellent wear-resistance, often under conditions where metals cold-weld. They are used as cutting and grinding tools, and for precision bearings in gyroscopes where no wear can be tolerated. When surfaces come into contact, the wear process begins at localized contact points where fracture, shearing, or flow takes place and small portions of the surface become debris. Adhesion and abrasion are involved in wear. The process by which ceramic materials wear differs from metallic wear owing to the brittleness and low surface energies of ceramics and carbides. Adhesive wear occurs only at elevated temperatures, about half the melting point or above, where plastic flow and adhesion take place. In most oxides, wear results from microfragmentation, sometimes visible to the eye but usually sub-microscopic. Fragmentation is caused by cleavage, intergranular fracture or fatigue cracking arising from impact or thermal shock during frictional heating.

High-speed sliding results in thermal spikes at the contact points, spikes which produce spark-like flashes of light in transparent materials. Abrasion is closely related to scratching, and materials with the same Mohs hardness should not abrade, but sliding velocity influences this simple relation. Frictional heating makes it possible to wear diamond with a high-speed rotating glass rod. High temperatures are generated by friction and maintained by poor thermal conductivity. High-speed tests on ceramics have shown that materials with low thermal conductivity and high thermal expansion wear fastest.

Surface roughness and crystal structure also influence friction. Friction is lowest for smooth surfaces where there is no interlocking of jagged peaks and where fluid films cover the surface. Single crystal studies show significant variations in frictional forces with crystallographic direction. Sliding in close-packed directions produces the lowest friction, although friction levels are generally high on all clean surfaces. Even graphite has high friction without adsorbed films on the exposed basal planes. Enormous increase in wear rates occur when the adsorbed layers of oxygen and water are removed from graphite platelets. Specially prepared carbon brushes for the electric generators of high-altitude aircraft are required for this reason.

Although much of the early experimental data is unreliable because of contaminating surface films, recent measurements in a vacuum environment have yielded reliable friction coefficients for single crystals. Friction is anisotropic and is generally lowest in planes of greatest packing density when sliding along closed packed directions. This is often true in ionic materials as well as in metals. In corundum, the coefficient of friction is smallest when sliding takes place on the close-packing (0001) plane and the sliding direction is [110]. In diamond friction is lowest for the tightly bonded (111) plane (Fig. 85).

The coefficient of friction is inversely proportional to cohesive energy, elastic modulus and hardness. The latter quantities decrease for the rocksalt series MgO, LiF, KCl, and KBr, while friction increases.

Frictional forces are associated with wear since high spots deform and shear when resisting tangential motion. The friction force is proportional to normal load and independent of the apparent contact area. However, most modern theories of friction are based on the idea that the true area of contact is proportional to load, making friction proportional to the shear area, $F = Sa$. The shear strength S can be controlled by surface conditions: a few layers of organic materials on a metal surface reduces frictional forces by an order of magnitude. Published frictional coefficients are highly questionable because of surface films, since even oxide coatings differ significantly. FeO and Fe_3O_4 are superior lubricants to Fe_2O_3 and cause a large variation in the frictional forces of hardened steel with oxygen pressure.

Solid lubricants provide a low-shear interface between bearing surfaces. Solids are used when other lubricants degrade or decompose at high temperature or under high radiation flux, and when fluids congeal at low temperatures or volatilize in high vacuums. Freedom from maintenance is another attractive feature, especially when bearing surfaces are inaccessible or run unattended. Solid lubricants are effective at high loads and slow speeds, but lack the self-healing and heat-dissipative qualities of fluid lubricants [39].

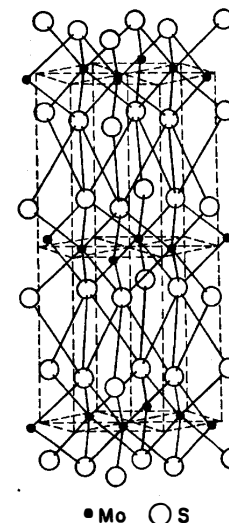


Fig. 86. The structure of molybdenite, MoS_2

Factors contributing to low shear strength include crystal structure, intercalated gases, and chemical interaction with the surfaces. Materials with lamellar crystal structures such as graphite and molybdenite (MoS_2) are effective lubricants because of slippage between planes (Fig. 86). Other sulfides and selenides of VIB elements such as NbSe_2 have been developed for electrical contact problems.

Not all solids with a lamellar structure have low-friction properties. TiS_2 has a structure similar to MoS_2 but is a poor lubricant, presumably because of relatively strong interlayer bonds. Talc is a better low-friction material than mica because of the weak van der Waals bonds between layers.

In addition to low shear strength, a good lubricant must have thermal stability, low vapor pressure, and oxidation resistance. It must form an adherent film to the substrate, a self-healing film with mobile adsorbate atoms to provide endurance. To avoid damaging metallic surfaces, the hardness of the lubricant is limited to about 5 on Mohs scale.

12. Dislocations and Plastic Deformation

Ionic crystals are less plastic than metals because dislocations are more difficult to form. Dislocations must be electrostatically-neutral. As a result, it is often necessary to remove two atomic layers instead of one

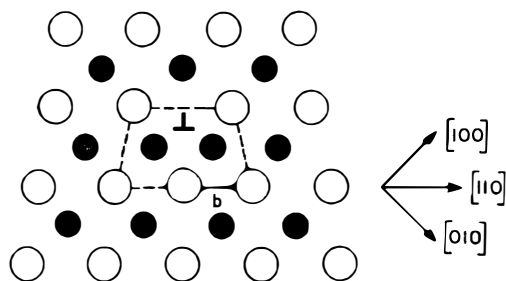


Fig. 87. Edge dislocation in NaCl showing the Burgers circuit (dashed line) and the Burgers vector b . Note that the enclosed cell has charge neutrality. The slip direction for the dislocation is $[110]$

as in a metal. An edge dislocation in rocksalt is illustrated in Fig. 87. The Burgers vector is the distance between next-nearest neighbors, rather than between nearest neighbors as in a metal. Dislocations with the smallest Burgers vector have the lowest strain energy and consequently will be the most likely to form.

The migration of dislocations is hindered by impurities which tend to collect near dislocations. The difference in size between impurity atoms and host atoms reduces the strain energy associated with the dislocation. Slip and plastic deformation is made more difficult because of the attractive forces between impurities and dislocations. CaCl_2 concentrations of 10^{-4} in NaCl are sufficient to double the yield stress.

An intimate relationship between deformation characteristics and crystal structure exists in aluminum oxide [40, 41]. No plastic deformation takes place below 1000°C . At higher temperatures, slip occurs within the close-packed (0001) plane. The minimum translation in the basal plane to give registry of the structure is about 5 \AA , a very large Burgers vector. In moving the dislocation, oxygen ions are required to move past other oxygens in the adjacent close-packed layer. This is accomplished by "partial" dislocation motion, avoiding direct superposition of the anions by zig-zag movements. Such complex dislocation structure requires synchronized movements of Al^{3+} and O^{2-} ions, which is possible only at high temperatures and low strain rates. Other slip systems are activated at still higher temperatures [42].

Dislocation formation and motion in covalent structures is also difficult. GILMAN [10] has discussed the crystallographic aspects of dislocations in diamond.

Metals have much less resistance to shear stresses than do most oxides. In oxides the repulsive forces between next nearest neighbors

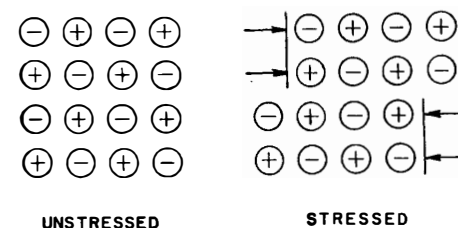


Fig. 88. Simple slip is difficult in ionic compounds because it usually brings ions of like charge into contact

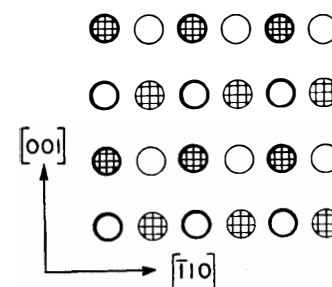


Fig. 89. The (110) plane of rocksalt is the preferred surface for mechanical glide. Glide takes place in the $[\bar{1}10]$ direction in which cations remain in contact with anions. In the drawing, sodium are cross-hatched circles and chlorines are open circles. Atoms in the upper plane are darker than those below

inhibits the slippage of one layer past another (Fig. 88). No such effect is present in pure metals where all neighbors are alike. The absence of slip in most ceramic materials not only makes them brittle but gives them great compressive strength as well.

In translation gliding the crystal shears like a deck of cards with a well-defined *translation glide plane* separating the displaced portions of the crystal. The *translation glide direction* is usually a simple crystallographic direction in which ion movement meets little resistance.

In halite (110) is the translation glide plane where $[\bar{1}10]$ and $[\bar{1}\bar{1}0]$ are the glide directions within this plane (Fig. 89). In translation gliding, the preferred planes and directions are such that Na^+ ions glide over Cl^- ions only, and *vice versa*, partially avoiding electrostatic repulsion. For the (110) plane this condition is met for the $[\bar{1}10]$ direction but not for $[001]$. When stressed in this orientation halite cleaves rather than

plastically deforming. $[110]$ gliding also takes place on the (100) and (111) planes of NaCl with the same line of argument holding true.

Slip lines are often observed on the surfaces of plastically-deformed metallic crystals. The lines are caused by the displacement of crystal planes, typically 1000 \AA . In close-packed metals—either hexagonal or cubic close-packed—slip occurs on the most densely packed planes. These are the most widely-separated planes in the crystal and therefore move past one another more easily.

In cubic close-packed (face-centered cubic) crystals the close-packed planes are the four $\{111\}$ planes. Within a given slip plane, the slip direction is the close-packed direction; for (111) the slip directions are $[1\bar{1}0]$, $[01\bar{1}]$, and $[\bar{1}01]$. Metallic deformation generally takes place *via* the slip plane and slip direction most nearly parallel to the applied stress. There are twelve slip systems (four planes and three directions in each) in FCC metals so that slip occurs rather easily.

The (00.1) planes are generally the slip planes in hexagonal close-packed metals. When c/a is considerably smaller, about 1.59, slip occurs on other planes as well. The slip directions are $\langle 110 \rangle$ for (00.1) planes, a total of only three slip systems for HCP metals.

Body-centered cubic metals show wavy slip lines, indicating that the slip systems are not well defined. The most important slip planes are the fairly densely populated $\{110\}$ planes.

Anisotropy in hardness is determined by crystal structure and the primary slip systems which accommodate dislocation motion during indentation. There is an inverse relationship between effective resolved shear stress in the region beneath the indenter and the observed hardness: directions corresponding to minimum shear stress are those of maximum hardness, and conversely. Isostructural compounds have similar slip systems therefore show similar hardness anisotropy, as shown in Table 24.

Table 24. Knoop hardness number measured on the (110) surface in various directions [43]

Solid	Structure	Measurement directions			Slip system
		$\langle 001 \rangle$	$\langle 1\bar{1}1 \rangle$	$\langle 1\bar{1}0 \rangle$	
MnS	NaCl	119	142	142	$\{110\} \langle 1\bar{1}0 \rangle$
LiF	NaCl	87	97	93	$\{110\} \langle 1\bar{1}0 \rangle$
MgO	NaCl	420	930	810	$\{110\} \langle 1\bar{1}0 \rangle$
Al	FCC	23	17	18	$\{111\} \langle 1\bar{1}0 \rangle$
Ni	FCC	115	84	84	$\{111\} \langle 1\bar{1}0 \rangle$
W	BCC	409	343	337	$\{123\} \langle 111 \rangle$
Nb	BCC	81	63	59	$\{123\} \langle 111 \rangle$
Fe	BCC	240	196	203	$\{123\} \langle 111 \rangle$

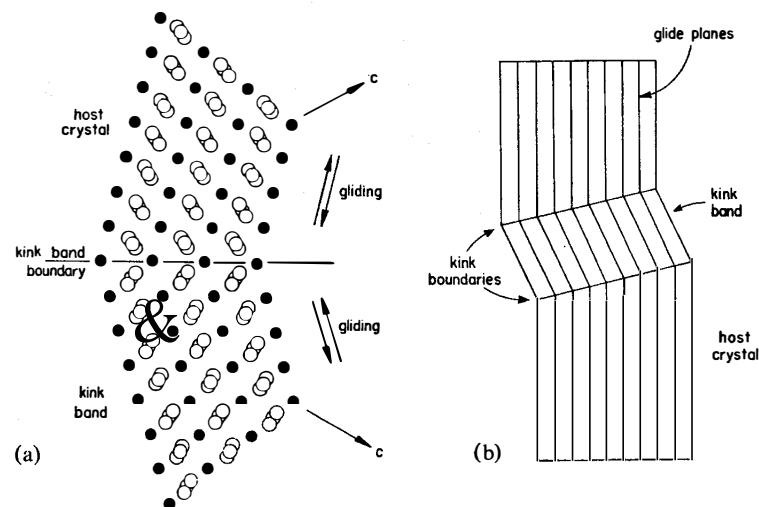


Fig. 90. (a) The boundary of a kink band in calcite. Carbonate groups are shown as open circles, calcium solid. (b) A single kink band

Kink bands are sharply defined zones in a crystal deformed by gliding, a type of ferroelastic behavior. Three types of kinking occur: 1. stress kinking, 2. kinking associated with a phase transformation, and 3. kinking caused by twin formation. As shown in Fig. 90, the zone boundaries are inclined to the active glide plane with the kink boundary bisecting the angle between the glide planes in the host crystal and in the kink band.

The active mechanism in *simple kinking* is translation gliding on a single line. Translation gliding occurs in mica, enstatite, and calcite. Calcite kinking takes place on $(10\bar{1}1)$ planes parallel to $[212]$, indexed on the morphological cell. The crystal structure of calcite at a kink boundary shown in Fig. 90 illustrated the atomic displacement accompanying kinking. Calcium ions translate and carbonate groups rotate so that the c -axis of the two segments are inclined by 52° . Since the sense of gliding on $(10\bar{1}1)$ is unique, as soon as a kink band forms, further gliding is arrested.

Phase transformations sometimes accompany gliding, creating kink bands with different crystal structure. Mechanical deformation converts enstatite into clinoenstatite. The host crystal is orthorhombic and the kink band monoclinic.

Twin gliding is responsible for the third type of kink band formation. In calcite twin gliding occurs on $(01\bar{1}2)$ and is closely controlled by the lattice geometry. Some of the complex deformation twinning in plagioclase feldspars also result from twin gliding [45].

13. Hard Metals

Strong alloys are required for cutting and grinding tools, and for turbine blades. Crystal chemistry plays an important role in many of the strengthening mechanisms. Among these mechanisms are *strain hardening*, *solid-solution hardening*, and *transformation hardening*.

Cold working introduces dislocations during plastic deformation to produce *strain hardening*. Yield strengths and hardening increase with rolling as the grains take on a preferred crystallographic orientation.

The martensitic transformation in Fe-C steels is the best example of *transformation hardening*. On cooling, iron undergoes a diffusionless phase transition from FCC to BCC. With a small amount of interstitial carbon, the BCC phase is distorted to tetragonal, becoming extremely hard and brittle. The laminar twin structure appearing at the transition contributes to the strengthening process.

Precipitation hardening can be very effective in systems in which the solid solution limit is a strong function of temperature. Generally the solid solubility of one phase in another increases with temperature. In the binary Al-Cu system, for instance, about 5 wt.-% Cu dissolves in Al near 550° C. At 300° C the solid solution limit is less than 1%. When an alloy containing 1-5% copper is rapidly quenched into the two-phase region, a finely dispersed precipitate is rejected from the supersaturated solid solution. Under appropriate heat-treatment conditions, several different transition structures may form in preference to the CuAl_2 equilibrium precipitate. Small clusters of copper atoms form when 4% Cu alloys are quenched and aged near room temperature. The plate-like clusters which are about 100 Å long and only two or three atoms thick, lie parallel to the $\{100\}$ planes of the aluminum host crystal. Sometimes referred to as *Guinier-Preston Zones*, the precipitated clusters are coherent with the host lattice such that Cu and Al atoms are in register along the interface between the two phases. Stress fields are developed in the vicinity of precipitate particles because of size mismatch between copper and aluminum atoms. The internal stresses impede the motion of dislocations, strengthening the alloy.

In *diffusion hardening*, a fine-grained precipitate is produced by reacting the metal with gases. Dispersed nitride or oxide particles increase wear resistance and surface hardness.

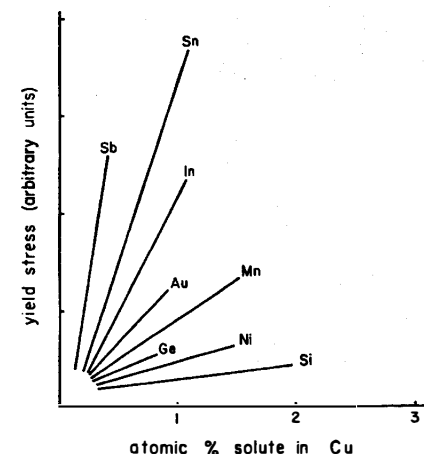


Fig. 91. Yield stress measurements on copper alloys. (After J.O. LINDE et al. [45])

Solution hardening, had its earliest application in the bronze age when tin was mixed in copper. Substitutional solute atoms produce lattice distortions which obstruct dislocation motion. Calculations of the shear strength based on atomic misfit predict the often-observed linear dependence of strength on composition (Fig. 91). The metallic radii for the solute elements shown are Sb (1.61 Å), Sn (1.59), In (1.58), Au (1.44), Mn (1.38), Ge (1.39), Ni (1.25), and Si (1.25). Comparing these values with Cu (1.28 Å) shows that those with largest radius difference produce the greatest misfit and therefore the greatest increase in yield stress.

Texture can also help strengthen materials to withstand greater mechanical stresses. The copper alloys used as springs in relays and connectors undergo a heavy rolling reduction to develop texture and greater strength. Yield strengths of various bronzes have been doubled without loss of ductility [45].

14. Cleavage

Cleavage is primarily determined by crystal structure and is only secondarily related to chemical composition. NaCl, MgO, PbS, and many other compounds with the rocksalt structure show easy cleavage parallel to the cubic $\{100\}$ faces. The crystal structure of CaCO_3 is a distorted variant of NaCl, and the characteristic cleavage rhombohedron of calcite also corresponds to the cleavage cube of rocksalt.

There are many excellent examples of cleavage among minerals. Muscovite, $\text{KAl}_2(\text{AlSi}_3\text{O}_{10})(\text{OH})_2$, can be cleaved into thin sheets, an

ideal geometry for parallel-plate capacitors. Muscovite is a member of the mica family, and like other layer silicates, cleavage takes place between silicate layers, breaking K–O bonds. Talc is a layer silicate which is used as a cosmetic. Its smoothness and covering power is related to gliding along the cleavage plane. Graphite is used in “lead” pencils for the same reason; the carbon layers rubbed from graphite crystals adhere strongly to paper. Both graphite and molybdenite (MoS_2) are excellent lubricants because of their easy cleavage. The plastic nature of clay so useful in shaping ceramics can be traced to sliding kaolin layers. Kaolinite [$\text{Al}_2\text{Si}_2\text{O}_5(\text{OH}_4)$] is a layer silicate with weak hydrogen bonds between aluminosilicate sheets.

Silicon-oxygen bonds are the strongest bonds in most minerals. Anisotropy in the silicate groups—as in the layer silicates—is generally responsible for cleavage. The pyroxenes and amphiboles are chain silicates with SiO_3 or Si_4O_{11} chains extending along the c -axis. Cleavage takes place along four $\{110\}$ planes parallel to the silicate chains. The angles between cleavage planes— 93° and 87° for pyroxenes, 124° and 56° for amphiboles—are useful diagnostic properties. Tremolite, $\text{Ca}_2\text{Mg}_5(\text{Si}_4\text{O}_{11})_2(\text{OH})_2$, and some of the other amphiboles are used as asbestos.

Topaz ($\text{Al}_2\text{SiO}_4\text{F}_2$) is an orthosilicate with perfect cleavage along (001). The structure consists of SiO_4 tetrahedra and AlO_4F_2 octahedra. Only Al–O and Al–F bonds are broken along the cleavage plane. The mineral cleaves between the silica tetrahedra leaving the stronger Si–O bonds intact. This is not so in feldspars. Orthoclase (KAlSi_3O_8) and the other feldspars are framework silicates with three-dimensional networks of interconnected SiO_4 and AlO_4 tetrahedra. There are, however, fewer bonds in some directions than in others, allowing the minerals to cleave along (001) and (010).

When more than one type of bonding is present, the weakest bonds are broken during cleavage. Gypsum ($\text{CaSO}_4 \cdot 2\text{H}_2\text{O}$) cleaves parallel to (010), breaking through a layer of hydrogen bonds and leaving the stronger ionic and covalent bonds intact.

Though quantitative measurements and quantitative theories are difficult, the observed cleavage directions in many simple salts can be explained by counting the number of broken bonds per unit area. As an example compare the relative cleavage energies of the three principal directions in fluorite, CaF_2 . Portions of the (111), (110) and (100) faces are illustrated in Fig. 92. Assigning an energy ϵ to each bond, the cleavage energy ϵ for a face may be estimated from the number of broken bonds per unit area. For fluorite the ratio of cleavage energies is $\epsilon_{100}:\epsilon_{110}:\epsilon_{111} = 1:\frac{1}{\sqrt{2}}:\frac{1}{\sqrt{3}}$. The cleavage energy is smallest for (111),

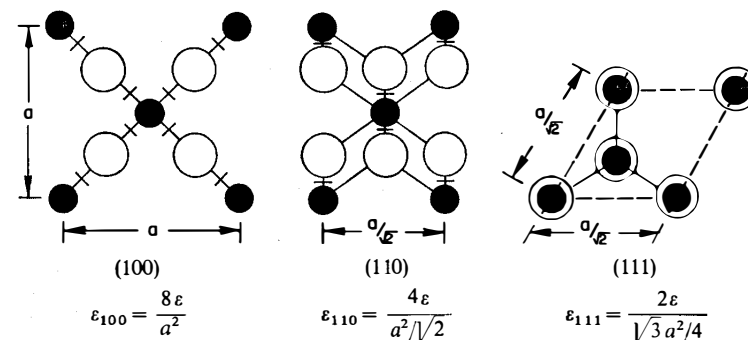


Fig. 92. Sections of the fluorite structure projected along [100], [110], and [111]. Bonds broken during cleavage are indicated

explaining why fluorite cleaves into regular octahedra. The simple model also explains the observed modes of cleavage in rock salt $\{100\}$ and diamond $\{111\}$.

Many objections can be raised to such a simple-minded theory of cleavage. In carrying out more precise theory for ionic surface energy calculations it is necessary to include long-range ionic forces, multipole forces due to polarizability (dipole-dipole and dipole-quadrupole terms), short-range repulsive forces and surface distortion energies. An excellent discussion of the calculations is given by Tosi [46]. For NaCl it is found that $\epsilon_{110}/\epsilon_{100} = 2.2$ and for CaF_2 , $\epsilon_{110}/\epsilon_{111} = 2.0$. Calculations on other alkali halides gave values between 2 and 3. These ratios are larger than those obtained by counting broken bonds: NaCl, $\epsilon_{110}/\epsilon_{100} = \sqrt{2}$ and CaF_2 , $\epsilon_{110}/\epsilon_{111} = \sqrt{3/2}$. Nevertheless, the elementary theory predicts the correct cleavage plane, and with slight modifications for relative bond energies, can be easily applied to more complicated crystal structures. A semi-quantitative understanding of cleavage in minerals then becomes possible. It is worth noting that the simple theory is expected to work best for materials with covalent or metallic bonds. The forces in ionic solids are long range by comparison. Calculations by RICHMAN [47] illustrate the application to metals. He included first- and second-nearest neighbor bonds in calculating the cleavage characteristics of Zn, Cd, Mg, and Be.

15. Brittle Fracture

All materials fracture under large tensile stresses but the separation takes a variety of forms. Rubber stretches enormously before tearing, ductile metals deform before breaking, while glass shows brittle behavior,

fracturing with little previous deformation. After brittle failure the fragments can (in principle) be reassembled to form the initial shape.

Brittle fracture is frequently catastrophic with rapid and unstable crack development. The crack travels in a direction normal to the main tensile stresses with relatively small energies expended, essentially the energy required to create new surface, about 10^3 erg/cm². Fracture velocities range from near zero to a limiting speed of about half the dilational stress wave velocity, approximately 5000 m/sec in MgO. Several authors contend that fracture speeds are limited to Rayleigh surface wave velocities which are also about half the bulk velocities [48]. Crystalline solids with well-defined cleavage planes have higher fracture velocities than glass and other isotropic materials.

Cleavage is a type of brittle fracture. In cleaving a crystal, it is desirable to produce a single crack with a smooth surface. The stone is notched parallel to the cleavage plane by continued rubbing, producing a groove, and a blunt wedge is inserted in the groove and tapped sharply to initiate cleavage. It is essential that the wedge should not reach the tip of the groove, but merely push sideways against the walls. In choosing the dimensions of the wedge, and in mounting the stone, it is desirable to avoid reflected waves and unwanted oscillations in the crack tip. An excessively energetic cleavage blow results in high fracture velocity and multiple fragmentation, a disaster in the diamond business.

16. Toughness

To be durable, a ceramic must be hard and tough to withstand abrasion and impact. *Hardness* means resistance to scratching, and *toughness* means resistance to breakage, whether by fracture, parting, or cleavage. Nephrite jade is a very tough material but it is not especially hard.

Hardness and toughness are physically irreversible properties since both tests leave the material in a permanently altered condition. Irreversible properties are defined in terms of a specific test which provides a numerical measurement indicative of the property under study. From the resulting numbers, materials can be ranked with regard to hardness or toughness, but the numbers have only a relative meaning since different tests lead to different scales.

Fracture energy is a measure of toughness. Bars are fractured in threepoint bend, integrating the resulting force-displacement curves to obtain the work of fracture. The experiment measures the work required to propagate a crack over a given cross-section, and is therefore expressed in ergs/cm². Surface fracture energies for several inorganic solids are

Table 25. Comparison of fracture surface energies. Fracture energies given in ergs/cm²

	Orientation	Fracture surface energy
Calcite	(10 $\bar{1}$ 1)	900
Corundum	(10 $\bar{1}$ 0)	600
Corundum	(11 $\bar{2}$ 3)	24000
Corundum	polycrystalline	40000
Fluorite	(111)	400
Halite	(100)	300
Jadeite	polycrystalline	120000
Kaolinite	polycrystalline	300
Muscovite	(001)	4000
Nephrite	polycrystalline	230000
Orthoclase	(001)	8000
Periclase	(100)	4000
Quartz	(11 $\bar{2}$ 0)	800
Quartz	(10 $\bar{1}$ 1)	500
Quartz	(10 $\bar{1}$ 0)	1000
Quartz	polycrystalline	4000

collected in Table 25. There is a lot of scatter in the data, reflecting the difficulty in achieving stable crack propagation in brittle materials, but it can be concluded that single crystals are not as tough as dense polycrystalline materials, and that the two jades, nephrite and jadeite, are toughest of all [49]. The toughness of jade makes it possible to carve extremely delicate forms without fracture, a fact so beautifully illustrated by Chinese artisans. It is interesting to note that jadeite (NaAlSi₂O₆, a pyroxene) and nephrite [Ca₂Mg₅Si₈O₂₂(OH)₂], are both chain silicates with excellent cleavage parallel to the chain directions. In polycrystalline materials, cleavage appears to enhance toughness rather than reduce it. Cleavage promotes transgranular fracture, creating a zig-zag fracture surface.

Most polycrystalline ceramic materials fracture along grain boundaries but in jadeite fracture proceeds directly through the grains in a transgranular fracture mode. At higher magnifications, cleavage step patterns are especially obvious, indicating that fractures are almost wholly restricted to certain crystallographic planes. The elongated nature of some of these cleavage steps strongly suggests that fractures occur parallel to the pyroxene chains, on the (110) and ($\bar{1}$ 10) planes. It is this extensive transgranular cleavage fracture mode that imparts toughness to jadeite.

Nephrite has a different fracture topography from jadeite. Fibers and bundles of fibers can be seen protruding from the nephrite fracture

surface even at low magnification. The random orientation of individual fibers leads to interlocking, increasing the fracture strength. Fibrous microstructure such as this occurs also in ballas diamond, a particularly tough variety of carbonado used in drilling rock.

There appear to be several mechanisms by which transgranular cleavage and fibrous microstructure might increase fracture energy. It seems almost contradictory to say that cleavage might enhance toughness. One thinks of mica and how easily the flakes are separated. But mica is a single crystal in which the cleavage planes extend from one edge of the specimen to the other. How does cleavage proceed in a polycrystalline material in which neighboring grains are oriented at random? Suppose a crack is propagated across a grain, following a cleavage plane. When the crack reaches a grain boundary where the crystal orientation changes, it changes direction and follows a cleavage plane in the second grain. In jadeite and nephrite, the (110) and ($\bar{1}10$) cleavage planes are parallel to the silicate chains. Since there are only two cleavage planes, the change in direction of the crack at the grain boundary can be quite substantial, up to 47° in jadeite and 62° in nephrite. A large change in crack direction might increase the work-to-fracture parameter for several reasons. First, the zig-zag fracture path results in a roughened surface, making the true surface area larger than the measured cross-sectional area. The increase in surface area is estimated to be about 50 percent, which is appreciable but not enough to account for the extraordinary work-to-fracture values found in jade. Branching is probably a more important factor. Because of the presence of two cleavage planes in each grain, crack-branching could occur at the grain boundaries, initiating two fracture surfaces in place of one. A large amount of energy could be dissipated in forming branched surfaces.

A third possible explanation as to why a large change in crack direction might increase the work-to-fracture is the pinning (impeding of motion) of cracks as the grain boundary surface. When a crack changes direction, various stress components at its tip must be enhanced to initiate fracture in the next grain. The stress buildup required for renucleation of the crack leads to larger forces and greater energy dissipation.

Yet another crack-pinning phenomenon may occur in nephrite, where the fibers are tightly interwoven. Cleavage planes are parallel to the fiber axis in nephrite so that cleavage occurs lengthwise, as in bamboo. The microstructure of nephrite resembles an interwoven mat of slender bamboo fibers. Under stress, a crack might develop in one bamboo fiber, splitting it lengthwise. As the crack approached the crossover point of a second bamboo fiber, it would be slowed and perhaps stopped until there was further increase in stress. This would increase the work-to-

fracture since larger stresses would be required to produce a given fracture surface. Frictional effects associated with the pulling out of fibers may also be important, but whatever the secret of its great strength, jade fully deserves its reputation as a very tough mineral.

17. Strengthening of Glass

Legend has it that the Roman Emperor Tiberius was shown a goblet of unbreakable glass whose owner proudly claimed to be the sole possessor of the secret of its manufacture. "If this art be propagated", the Emperor said, "gold and silver will become of no more value than dirt". He then ordered the craftsman to be put to death so that the secret would die with its owner. Fortunately present-day glass manufacturers have more enlightened personnel policies.

Windshield safety glass for automobiles is toughened and laminated to prevent injuries. Laminated glass consists of two layers of glass bonded to a central layer of transparent plastic. Polyvinyl butyral interlayers are excellent energy-absorbers, with about 400% elongation before failure. The role of the interlayer is to arrest forward movement, preventing laceration and penetration of the windshield.

Another practical way to strengthen glass is to put the surface into compression. Both thermal and chemical techniques are used in *surface-compression strengthening*. Thermal quenching or tempering is accomplished by cooling the exterior of hot glass with air jets or with liquids. The ultimate limit for this type of process is determined by the steepness of the temperature gradient which can be sustained as the glass cools through the strain point. Thermal strengthening of polycrystalline ceramics can also be accomplished by quenching. It is necessary to heat the ceramic enough to promote rapid plastic creep, which is equivalent to the viscous deformation important in the tempering of glass.

There are two kinds of chemical strengthening. The simplest way is to force extra atoms or molecules into the surface of the glass. Fused silica can be strengthened by impregnating the surface with argon. A more practical technique is ion exchange, replacing small ions with large ions. Substantial strengthening of soda-lime glass is achieved by immersion in fused potassium nitrate. Large K^+ ions from the melt exchange positions with smaller Na^+ ions in the glass, placing the surface under compression. Aluminosilicate glasses equilibrate more rapidly than silica glasses because there are fewer nonbridging oxygens to inhibit exchange of alkali ions. Potassium-lithium substitution is more effective than potassium-sodium because of the greater size difference. Scratch-resistant glasses are produced in this way.

A second type of chemical strengthening is based on control of the thermal expansion coefficients of the surface and bulk. If the surface has a lower coefficient, the surface is compressed when the glass is cooled from high temperature. Low values of α are obtained by dealcalization of a soda-lime glass by heating in moist SO_2 , or by selective crystallization of a low-expansion phase such as β -eucryptite on the surface.

Composites made of polymer-bonded glass fibers exhibit impressive strength-to-weight ratios. Glass filaments are strong because of the absence of plastic deformation and surface irregularities which initiate cracks. Smooth surfaces are produced on drawing the fiber from molten glass, and protected by a plastic coating. The minimum stress σ required to propagate a sharp crack in a brittle material is given by the Griffith equation:

$$\sigma = \sqrt{\frac{4\gamma E}{\pi l}},$$

γ is the surface energy of newly-formed surface, l is length of the crack, and E is Young's modulus. For glass, γ is about 10^3 ergs/cm² and E about 10^{12} dynes/cm². Crack lengths in fibers with atomically-smooth surfaces do not exceed a few angstroms whereas incipient fractures in bulk glass are micron-size. Fracture stresses of 3×10^{11} dynes/cm² for fibers, and 3×10^9 for bulk glass are computed from the Griffith equation. The results are comparable to observed values and point out the importance of surface preparation.

Atomically-smooth surfaces have been produced in fibers as large as several millimeters in diameter. Glass has an important advantage over metals in regard to mechanical properties. Plastic deformation occurs by dislocation movement in most crystalline solids, but dislocations cannot exist in the aperiodic structure of glass, one of the strongest engineering materials available.

18. Composite Materials

Composite materials are composed of a mixture of phases in which the properties of one component enhance those of another. They generally consist of a matrix material reinforced with fibers, flakes or particles [50, 51]. Familiar examples include reinforced concrete (quartz aggregate and steel rods embedded in Portland cement) and fiber-glass (glass fibers surrounded by a plastic matrix). Laminated materials such as plasterboard and plywood are a different type of composite.

Table 26. Typical properties of reinforcement filaments

Continuous filaments	Density	Tensile strength	Elastic modulus
Silica glass	2.19 (g/c.c.)	60×10^3 kg/cm ²	0.7×10^6 kg/cm ²
Boron	2.63	32	4.1
Silicon carbide	3.35	28	4.6
Alumina	3.96	28	4.7
Carbon	1.90	22	3.5
Beryllium	1.83	13	2.5
Steel	7.70	42	2.0
Tungsten	19.4	42	4.2

The properties of the constituents influence the performance of the composite. Some properties such as the density are simply the average of those of the components, but in other cases the composite is superior to either component. A second phase may inhibit dislocation motion, giving rise to high strength materials. Tungsten carbide, a cermet, is used extensively as a cutting tool. Another cermet, tungsten-thoria is used as a lamp filament. A dispersion of ThO_2 in Ni gives a composite several times stronger than pure nickel.

Metal-matrix composites are primarily of interest for aerospace applications where high costs can be justified by high performance. Very fine whiskers have the highest strengths yet obtained, but the cost and difficulty of incorporating them into useful shapes have eliminated them from most practical applications. The greatest emphasis has been placed on developing continuous filaments with high stiffness, high strength and low density (Table 26). In fabricating a composite body, a lathe is used to drum-wind the filament over the matrix metal foil and the two are bonded together by a plasma-sprayed matrix alloy. The final shape is cut from the monolayer, stacked, and hot-pressed. The bonding problem is aggravated by a serious thermal expansion mismatch between metal and fiber.

Directionally-solidified eutectics (DSE) are a class of thermodynamically-compatible composites made from eutectic compositions. A temperature gradient is used to produce directional solidification. The two phases freeze simultaneously with either whisker-like rods or lamellae of one phase forming within the other, forming an anisotropic composite, and imparting great strength to the material. DSE composites of Ni_3Al - Ni_3Nb have been used as coated turbine vanes. Ni - NbC , Co - TaC , and other refractory metals reinforced with carbides are another group of eutectics under investigation.

References for Chapter VII

1. BECHMANN, R., HEARMON, R. F. S., KURTZ, S. K.: Landolt-Börnstein, New Series Group III, Vols. 1, 2. Berlin-Heidelberg-New York: Springer 1966, 1969.
2. SIMMONS, G.: J. Grad. Res. Center, Southern Methodist University, **34**, 1 (1965).
3. HUNTINGDON, H. B.: Solid State Physics, Vol. 7, p. 214 (eds. F. SEITZ and D. TURNBULL). New York: Academic Press 1958.
4. BIRCH, F.: J. Geophys. **4**, 295 (1961).
5. BIRCH, F.: J. Geophys. Res. **66**, 2199 (1961).
6. SIMMONS, G.: J. Geophys. Res. **69**, 1123 (1964).
7. PINNOW, D. A.: Trans. I.E.E.E. QE-6, 223 (1970).
8. MEYER, A., UMAR, I. H., YOUNG, W. H.: Phys. Rev. B **4**, 3287 (1971).
9. ANDERSON, O., NAFE, J. E.: J. Geophys. Res. **70**, 3951 (1965).
10. GILMAN, J. J.: The Physics and Chemistry of Ceramics, p. 240 (ed. C. KLINGSBERG). New York: Gordon and Breach 1963.
11. KITTEL, C.: Introduction to Solid State Physics, First Edition, p. 53. New York: John Wiley and Sons 1953.
12. MATOSI, F.: J. Chem. Phys. **17**, 679 (1949).
13. HIDALGO, A., SERRATOSA, J. M.: Chem. Abstr. **50**, 10532gh (1956).
14. NYQUIST, R. A., KAGEL, R. O.: Infrared Spectra of Inorganic Compounds. New York: Academic Press 1971.
15. WILSON, E. B., DECIUS, J. C., CROSS, P. C.: Molecular Vibrations. New York: McGraw-Hill Book Co. 1955.
16. SUTTON, L. E.: Tables of interatomic distances and configuration in molecules and ions, Special publication II. London: The Chemical Society 1958.
17. MAKASHIMA, A., MACKENZIE, J. Non-Cryst. Solids **12**, 35 (1973).
18. CHUNG, D. H., BUESSEM, W. R.: Anisotropy in single-crystal refractory compounds, Vol. 2, p. 217 (eds. F. VAHLIDIEK and S. A. MERSOL). New York: Plenum Press 1958.
19. WEIDNER, D. J., SIMMONS, G.: J. Geophys. Res. **77**, 826 (1972).
20. NEWNHAM, R. E., YOON, H. S.: Mineral. Mag. **39**, 78 (1973).
21. YOON, H. S., NEWNHAM, R. E.: Acta Cryst. A **29**, 507 (1973).
22. MCSKIMIN, H. J., ANDREATCH, P., THURSTON, R. N.: J. Appl. Phys. **36**, 1624 (1965).
23. GEISKE, J. H., BARSCH, G. R.: Phys. Stat. Sol. **29**, 121 (1968).
24. GRAHAM, E. K., BARSCH, G. R.: J. Geophys. Res. **74**, 5949 (1969).
25. CARR, P. H., DEVITO, P. A., SZABO, T. L.: Trans. I.E.E.E. SU-19, 357 (1972).
26. MEGAW, H.: Mat. Res. Bull. **6**, 1007 (1971).
27. HUMMEL, F. A.: J. Am. Ceram. Soc. **33**, 102 (1950).
28. TAYLOR, D.: Mineral. Mag. **28**, 593 (1972).
29. DEER, W. A., HOWIE, R. A., ZUSSMANN, J.: Rock forming minerals, Vol. 4. New York: John Wiley and Sons. 1963.
30. BELL, R. O., RUPPRECHT, G.: Phys. Rev. **129**, 90 (1963).
31. AXE, J. D.: Trans. Am. Cryst. Assoc. **7**, 89 (1971).
32. PRICE, C. C.: J. Chem. Ed. **50**, 744 (1973).
33. ALLCOCK, H. R.: Sci. Am. **230**, 66 (1974).
34. JENSEN, A. T.: Arkiv f. Kemi **30**, 165 (1968).
35. PLENDL, J. N., GIELISSE, P. J.: Zeit. Krist. **118**, 404 (1963).
36. PETERS, C. G., NEFFLEN, K. F., HARRIS, F. K.: N. B. S. J. Res. **34**, 587 (1945).
37. BEAN, K. E., GLEIM, P. S.: Proc. I.E.E.E. **57**, 1469 (1969).
38. RABINOWICZ, E.: Science J. **6**, 45 (1970).
39. JENTGEN, R. L.: Trans. I.E.E.E. PHP-7, 86 (1971).

40. KRONBERG, M. L.: Acta Met. **5**, 507 (1957).
41. KINGERY, W. D.: Introduction to ceramics. New York: John Wiley and Sons 1960.
42. SNOW, J. D., HEUER, A. H.: J. Am. Ceram. Soc. **56**, 153 (1973).
43. BROOKS, C. A., O'NEILL, J. B., REDFERN, B. A. W.: Proc. Roy. Soc. A **322**, 73 (1971).
44. STARKEY, J.: Contr. Min. and Pet. **19**, 133 (1968).
45. LINDE, J. O., LINDELL, B. O., STADE, C. H.: Arkiv Fysik **2**, 89 (1950).
46. TOSI, M. P.: Solid State Physics, Vol. 16, p. 1 (eds. F. SEITZ and D. TURNBULL). New York: Academic Press 1964.
47. RICHMAN, M. H.: Trans. A. S. M. **59**, 374 (1966).
48. FIELD, J. E.: Contemp. Phys. **12**, 1 (1971).
49. BRADT, R. C., NEWNHAM, R. E., BIGGERS, J. V.: Am. Mineralogist **58**, 727 (1973).
50. HOLLIDAY, L.: Composite materials. New York: American Elsevier Publishing Co. 1966.
51. BROUTMAN, L. J., KROCK, R. H.: Modern composite materials. Reading, Mass.: Addison-Wesley Publishing Co. 1967.